

Magnetostrictive Rare Earth- Fe_2 Compounds

A.E. Clark

Naval Surface Weapons Center, White Oak Laboratory,
Silver Spring, MD 20910, USA

1. Introduction

By the early 1960's, it was widely recognized that the rare earths possessed many extraordinary magnetic properties. Neutron diffraction measurements, for example, showed that the spin structures were much more complex than those of any of the classical ferromagnets or antiferromagnets. More importantly, in the heavy rare earth metals, the parallel coupling of large orbital and large spin angular momenta yielded huge magnetic moments of $9\mu_B$ and $10\mu_B$, dwarfing the conventional values of 0.6 for Ni and 2.2 for Fe. Enormous magnetic anisotropies were also encountered in the heavy rare earth elements. In 1963, a breakthrough in magnetostrictive materials occurred with the measurement of the basal plane magnetostrictions of Tb and Dy at low temperatures (Legvold et al. 1963, Clark et al. 1963, 1965, Rhyne and Legvold 1965). These basal plane strains are 100 to 10000 times typical magnetostrictions and still remain today the largest known ($\sim 1\%$). Over wide temperature ranges, thermal expansions are dominated by the temperature dependences of the magnetostrains. Elastic moduli were found to be strongly influenced by the unprecedented magnetoelastic interactions. However, because of the low ordering temperatures of the rare earths the application of these magnetostrictive properties to devices operating at room temperature could not be achieved with the elements. Only Gd, which is essentially non-magnetostrictive, possesses a Curie point as high as room temperature.

In 1971 a search for magnetostrictive materials with high magnetostriction at room temperature was started. Highly magnetostrictive rare earths, Tb and Dy, were combined with the magnetic transition metals, Ni, Co and Fe, by direct compound synthesis and by rapid sputtering into amorphous alloys. The cobalt rich $R_2\text{Co}_{17}$ compounds (R = rare earth) possess Curie temperatures as high as 1200 K, and exhibit moderate magnetostrictions at room temperature. The remaining Co compounds, which are richer in rare earths, plus all the Ni compounds, possess lower ordering temperatures and very low room temperature magnetostrictions. In contrast to the normal Curie temperature behavior of the Ni and Co compounds, the Curie temperatures of the rare earth-iron compounds *increase* with increasing rare earth concentration. The highest ordering temperatures are found for the Laves phase $R\text{Fe}_2$ compounds. Both the high concentration of rare earth and the high Curie temperatures of

these compounds are responsible for huge room temperature magnetostrictions in $TbFe_2$ and in $SmFe_2$. Non-crystalline Tb_xFe_{1-x} ($x \approx \frac{1}{2}$) alloys also possess comparatively high Curie temperatures and large room temperature magnetostrictions.

Magnetic anisotropy plays an important role in magnetostrictive materials. First, it is important to recognize that there is no linear magnetostriction if the anisotropy is independent of the state of strain of the crystal. In effect, the crystal deforms spontaneously whenever to do so lowers the anisotropy energy. On the other hand, the existence of magnetic anisotropy itself may be a hindrance to the technical usefulness of a magnetostrictive material. Large fields may be required to attain the large magnetostriction. In fact, $TbFe_2$ possesses an anisotropy energy $> 10^7$ ergs/cm³ and an anisotropy field > 100 kOe, about two orders of magnitude larger than that of conventional cubic metals.

In addition to the conventional static magnetoelastic property (i.e. magnetostriction), elastic phenomena, both static and dynamic can be dominated by magnetoelastic effects. Elastic constants in single crystal RFe_2 compounds are modified by as much as 60% by the strong magnetoelastic interaction. In polycrystal and amorphous alloys, the high symmetry of cubic and isotropic samples is clearly broken. In $Sm_{0.88}Dy_{0.12}Fe_2$, the degeneracy between shear waves is removed by the magnetoelastic coupling producing two shear modes whose moduli differ by 30%.

This chapter presents an overview of the magnetoelastic properties of the highly magnetostrictive rare earth- Fe_2 alloys. In section 2 a general treatment of magnetostriction is given for the cases of hexagonal and cubic symmetry, which is applicable to the rare earth elements and the rare earth-iron compounds. The expressions for the magnetostriction up to sixth order in the direction cosines of the magnetization are given in Appendix A. In section 3 the magnetostriction of binary rare earth-iron alloys is presented. The magnetostriction of single crystal and polycrystal RFe_2 compounds are compared to other magnetostrictive materials at room temperature. A possible source of a startling magnetostriction anisotropy ($\lambda_{111} \gg \lambda_{100}$) is discussed. Magnetization, sublattice magnetization and magnetic anisotropy measurements are presented in sections 4 and 5. Measurements on single crystals are compared to those on polycrystals. In section 6 the magnetostrictive properties of pseudobinary Tb -based and Sm -based RFe_2 alloys are examined. The effects of the strong magnetoelastic coupling on sound velocities and elastic moduli are reported in sections 7 and 8. Extraordinarily large ΔE effects and changes in sound velocity are observed in single crystals, polycrystals and amorphous rare earth- Fe_2 alloys. The role of intrinsic (intra-domain) as well as extrinsic (domain wall induced) effects are discussed. Low signal linear transduction properties of certain highly magnetostrictive materials are given in section 8. Finally, in section 9, recent measurements of linear and volume magnetostriction on the amorphous form of the RFe_2 alloys are presented.

The objective of this chapter is to focus on the magnetostrictive RFe_2 alloys. For a broad review of the magnetic properties of the rare earth-transition metal alloys, the reader is referred to chapters 3 and 4 of this volume and references therein.

2. Phenomenology of magnetostriction

Akulov (1928) and Becker and Döring (1939) developed simple expressions to describe the magnetostriction of cubic crystals. A commonly accepted expression, utilizing five constants, has the form

$$\begin{aligned}\Delta l/l = & h_1(\alpha_x^2\beta_x^2 + \alpha_y^2\beta_y^2 + \alpha_z^2\beta_z^2 - \frac{1}{3}) \\ & + 2h_2(\alpha_x\alpha_y\beta_x\beta_y + \alpha_y\alpha_z\beta_y\beta_z + \alpha_z\alpha_x\beta_z\beta_x) \\ & + h_4(\alpha_x^4\beta_x^2 + \alpha_y^4\beta_y^2 + \alpha_z^4\beta_z^2 + \frac{2}{3}s - \frac{1}{3}) \\ & + 2h_5(\alpha_x\alpha_y\alpha_z^2\beta_x\beta_y + \alpha_y\alpha_z\alpha_x^2\beta_y\beta_z + \alpha_z\alpha_x\alpha_y^2\beta_z\beta_x) \\ & + h_3s \quad [\text{or } h_3(s - \frac{1}{3})].\end{aligned}\quad (2.1)$$

Here α_i denote the direction cosines of the magnetization with respect to the crystal axes; β_i the direction cosines of the measurement direction with respect to the crystal axes, and $s = \alpha_x^2\alpha_y^2 + \alpha_y^2\alpha_z^2 + \alpha_z^2\alpha_x^2$.

Frequently the magnetostriction is empirically fitted by the two lowest order terms. Denoting by λ_{100} the change in length along [100] when the magnetization is also in that direction, and by λ_{111} the change in length along [111] when the magnetization is along [111], the magnetostrictive strain reduces to

$$\begin{aligned}\Delta l/l = & \frac{1}{2}\lambda_{100}(\alpha_x^2\beta_x^2 + \alpha_y^2\beta_y^2 + \alpha_z^2\beta_z^2 - \frac{1}{3}) \\ & + 3\lambda_{111}(\alpha_x\alpha_y\beta_x\beta_y + \alpha_y\alpha_z\beta_y\beta_z + \alpha_z\alpha_x\beta_z\beta_x).\end{aligned}\quad (2.2)$$

In the special case of an isotropic body (whether polycrystal or amorphous)

$$\Delta l/l = \frac{1}{2}\lambda_i(\cos^2\theta - \frac{1}{3}) \quad (2.3)$$

where θ denotes the angle between the magnetization and the measurement direction.

The linear magnetostriction described here originates because the magnetic anisotropy energy depends upon strain. The crystal therefore deforms to minimize the total energy. In the following, the general form of the magnetostriction for both cubic and hcp systems is derived. The cubic expressions are appropriate for many metals, including the RT_2 and R_6T_{23} rare earth (R) transition metal (T) compounds. The hexagonal expressions apply to RT_3 , R_2T_{17} and to many of the rare earth elements.

The total energy must be invariant under the symmetry operations of the crystal lattice. It can conveniently be written

$$E = E_0 + E_a + E_{me} + E_{el}. \quad (2.4)$$

E_0 denotes the part of the magnetic energy which is independent of magnetization direction. E_a , the anisotropy energy, can be expressed in terms of polynomials of the direction cosines which transform according to the fully symmetric representation of the crystal, i.e. the cubic or hexagonal harmonics. These polynomials are listed in table 1 (Bell 1954). The polynomials which keep the crystal symmetry intact are identified by α . Letting $K^{\alpha\beta}$ denote the anisotropy constants and $S^{\alpha\beta}$, the symmetry polynomials

TABLE 1
Basis functions for cubic and hexagonal lattices (taken from Bell 1954)

	Cubic	Hexagonal
$S_{\gamma}^{a,0}$	$\alpha_x^2 + \alpha_y^2 + \alpha_z^2 = 1$	$S_{\gamma}^{a,0}$ $\alpha_x^2 + \alpha_y^2 + \alpha_z^2 = 1$
$S_{\gamma}^{a,2}$	$\frac{1}{2}(2\alpha_x^2 - \alpha_y^2 - \alpha_z^2)$	$S_{\gamma}^{a,2}$ $\alpha_x^2 - \frac{1}{3}$
$S_{\gamma}^{a,2}$	$(\sqrt{3}/2)(\alpha_x^2 - \alpha_y^2)$	$S_{\gamma}^{a,2}$ $\frac{1}{2}(\alpha_x^2 - \alpha_y^2)$
$S_{\gamma}^{a,2}$	$\alpha_x \alpha_z$	$S_{\gamma}^{a,2}$ $\alpha_x \alpha_y$
$S_{\gamma}^{a,2}$	$\alpha_x \alpha_z$	$S_{\gamma}^{a,2}$ $\alpha_x \alpha_z$
$S_{\gamma}^{a,2}$	$\alpha_x \alpha_y$	$S_{\gamma}^{a,2}$ $\alpha_x \alpha_y$
$S_{\gamma}^{a,4}$	$\alpha_x^4 + \alpha_y^4 + \alpha_z^4 - \frac{1}{3}$	$S_{\gamma}^{a,4}$ $\alpha_x^4 - \frac{6}{5}(\alpha_x^2 - \frac{1}{3}) - \frac{1}{3}$
$S_{\gamma}^{a,4}$	$2\alpha_x^4 - \alpha_y^4 - \alpha_z^4 - \frac{6}{5}(2\alpha_x^2 - \alpha_y^2 - \alpha_z^2)$	$S_{\gamma}^{a,4}$ $\frac{1}{5}(\alpha_x^2(\alpha_x^2 - \alpha_y^2) - \frac{1}{5}(\alpha_x^2 - \alpha_y^2))$
$S_{\gamma}^{a,4}$	$\sqrt{3}((\alpha_x^2 - \alpha_y^2) - \frac{6}{5}(\alpha_x^2 - \alpha_z^2))$	$S_{\gamma}^{a,4}$ $\alpha_x^2 \alpha_y - \frac{1}{5} \alpha_x \alpha_z$
$S_{\gamma}^{a,4}$	$\alpha_x^2 \alpha_z - \frac{1}{5} \alpha_x \alpha_y$	$S_{\gamma}^{a,4}$ $\frac{1}{5}(\alpha_x^4 - 6\alpha_x^2 \alpha_y^2 + \alpha_z^4)$
$S_{\gamma}^{a,4}$	$\alpha_x^2 \alpha_z - \frac{1}{5} \alpha_x \alpha_y$	$S_{\gamma}^{a,4}$ $(\alpha_x^2 - \alpha_y^2) \alpha_x \alpha_z$
$S_{\gamma}^{a,4}$	$\alpha_y^2 \alpha_z - \frac{1}{5} \alpha_x \alpha_y$	$S_{\gamma}^{a,4}$ $\alpha_x^3 \alpha_z - \frac{1}{5} \alpha_x \alpha_z$
$S_{\gamma}^{a,6}$	$\alpha_x^2 \alpha_y^2 \alpha_z^2 + \frac{1}{15}(\alpha_x^4 + \alpha_y^4 + \alpha_z^4 - \frac{1}{3}) - \frac{1}{105}$	$S_{\gamma}^{a,6}$ $\alpha_x^6 - \frac{15}{11}(\alpha_x^4 - \frac{6}{5}(\alpha_x^2 - \frac{1}{3}) - \frac{1}{3}) - \frac{6}{5}(\alpha_x^2 - \frac{1}{3}) - \frac{1}{3}$
$S_{\gamma}^{a,6}$	$2\alpha_x^6 - \alpha_y^6 - \alpha_z^6 - \frac{15}{11}(2\alpha_x^4 - \alpha_y^4 - \alpha_z^4) - \frac{6}{5}(2\alpha_x^2 - \alpha_y^2 - \alpha_z^2) - \frac{6}{5}(\alpha_x^2 - \alpha_y^2 - \alpha_z^2))$	$S_{\gamma}^{a,6}$ $\alpha_x^6 - 15\alpha_x^4 \alpha_y^2 + 15\alpha_x^2 \alpha_y^4 - \alpha_y^6$
$S_{\gamma}^{a,6}$	$\sqrt{3}(\alpha_x^6 - \alpha_y^6 - \frac{15}{11}(\alpha_x^4 - \alpha_y^4 - \frac{6}{5}(\alpha_x^2 - \alpha_y^2))) - \frac{6}{5}(\alpha_x^2 - \alpha_y^2))$	$S_{\gamma}^{a,6}$ $\frac{1}{5}(\alpha_x^4 - \frac{6}{11}(\alpha_x^2 - \frac{1}{3}) - \frac{1}{21})(\alpha_x^2 - \alpha_y^2)$
$S_{\gamma}^{a,6}$	$(\alpha_x^4 - \frac{6}{11}(\alpha_x^2 - \frac{1}{3}) - \frac{1}{21})\alpha_x \alpha_z$	$S_{\gamma}^{a,6}$ $(\alpha_x^4 - \frac{6}{11}(\alpha_x^2 - \frac{1}{3}) - \frac{1}{21})\alpha_x \alpha_y$
$S_{\gamma}^{a,6}$	$(\alpha_y^4 - \frac{6}{11}(\alpha_y^2 - \frac{1}{3}) - \frac{1}{21})\alpha_x \alpha_z$	$S_{\gamma}^{a,6}$ $\frac{1}{5}(\alpha_x^2 - \frac{1}{11})(\alpha_x^4 - 6\alpha_x^2 \alpha_y^2 + \alpha_z^4)$
$S_{\gamma}^{a,6}$	$(\alpha_z^4 - \frac{6}{11}(\alpha_z^2 - \frac{1}{3}) - \frac{1}{21})\alpha_x \alpha_y$	$S_{\gamma}^{a,6}$ $(\alpha_x^2 - \frac{1}{11})(\alpha_x^2 - \alpha_y^2) \alpha_x \alpha_z$
$S_{\gamma}^{a,6}$	$(\alpha_x^4 + \alpha_y^4 - \frac{10}{3}\alpha_x^2 \alpha_y^2)\alpha_x \alpha_z$	$S_{\gamma}^{a,6}$ $(\alpha_x^4 - \frac{10}{11}(\alpha_x^2 - \frac{1}{3}) - \frac{1}{21})\alpha_x \alpha_z$
$S_{\gamma}^{a,6}$	$(\alpha_x^4 + \alpha_y^4 - \frac{10}{3}\alpha_x^2 \alpha_y^2)\alpha_x \alpha_z$	$S_{\gamma}^{a,6}$ $(\alpha_x^4 - 10\alpha_x^2 \alpha_y^2 + 5\alpha_z^4)\alpha_x \alpha_z$
$S_{\gamma}^{a,6}$	$(\alpha_x^4 + \alpha_y^4 - \frac{10}{3}\alpha_x^2 \alpha_y^2)\alpha_x \alpha_y$	$S_{\gamma}^{a,6}$ $(5\alpha_x^4 - 10\alpha_x^2 \alpha_y^2 + \alpha_z^4)\alpha_x \alpha_y$

$$E_a = \sum_i K^{a,i} S^{a,i}.$$

To lowest degree in α :

$$E_a|_{\text{cubic}} = K^{a,4}(\alpha_x^4 + \alpha_y^4 + \alpha_z^4 - \frac{1}{3}), \quad \text{or}$$

$$= K_1(\alpha_x^2 \alpha_y^2 + \alpha_y^2 \alpha_z^2 + \alpha_z^2 \alpha_x^2) + \text{constant} \quad (2.5a)$$

and

$$E_a|_{\text{hex}} = K^{a,2}(\alpha_z^2 - \frac{1}{3}). \quad (2.5b)$$

The magnetoelastic energy, E_{me} , arises from the strain dependence of the anisotropy energy and for small strains takes the form: $E_{me} \sim ef(\alpha)$. This term, in order to possess the correct transformation properties of the crystal, must be a direct product of strain components and direction cosine polynomials which transform according to the same symmetry representation (Callen and Callen 1963). In the cubic system the symmetry strain components fall into the three irreducible representations given in table 2 and designated by α , γ , and ϵ . The subscript denotes the components of the same irreducible representation. In the hexagonal system, the strain components consist of two fully symmetric components, designated by α_1 and α_2 , and two 2-dimensional representations γ and ϵ .

Thus taking the direct product of the symmetry strains and the direction

TABLE 2
Symmetry strain components for cubic and hexagonal lattices

	Cubic	Hexagonal
ϵ^a	$\epsilon_{xx} + \epsilon_{yy} + \epsilon_{zz}$	$\epsilon^{a1} = \epsilon_{xx} + \epsilon_{yy} + \epsilon_{zz}$
ϵ^γ	$\frac{1}{2}(2\epsilon_{zz} - \epsilon_{xx} - \epsilon_{yy})$	$\epsilon^{a2} = \frac{1}{2}(2\epsilon_{zz} - \epsilon_{xx} - \epsilon_{yy})$
ϵ_2^z	$(\sqrt{3}/2)(\epsilon_{xx} - \epsilon_{yy})$	$\epsilon_1^\gamma = \epsilon_{xx} - \epsilon_{yy}$ *
ϵ_1^x	ϵ_{yy}	$\epsilon_2^\gamma = \epsilon_{xy}$
ϵ_2^x	ϵ_{zz}	$\epsilon_1^x = \epsilon_{yz}$
ϵ_3^y	ϵ_{xy}	$\epsilon_2^x = \epsilon_{zx}$

* In this table the strains are defined by $\Delta x = \epsilon_{xx}x + \frac{1}{2}\epsilon_{xy}y + \frac{1}{2}\epsilon_{xz}z$. Note: $\epsilon_1^\gamma = \frac{1}{2}(\epsilon_{xx} - \epsilon_{yy})$ if the strains were defined by $\Delta x = \epsilon_{xx}x + \epsilon_{xy}y + \epsilon_{xz}z$.

cosine polynomials, E_{me} becomes

$$E_{me}|_{\text{cubic}} = \sum_l [B^{a,l} \epsilon^a S^{a,l} + B^{\gamma,l} \sum_i \epsilon_i^\gamma S_i^{\gamma,l} + B^{e,l} \sum_i \epsilon_i^e S_i^{e,l}] \quad (2.6a)$$

$$E_{me}|_{\text{hex}} = \sum_l [B^{a1,l} \epsilon^{a1} S^{a1,l} + B^{a2,l} \epsilon^{a2} S^{a2,l} + B^{\gamma,l} \sum_i \epsilon_i^\gamma S_i^{\gamma,l} + B^{e,l} \sum_i \epsilon_i^e S_i^{e,l}]. \quad (2.6b)$$

In terms of the conventional cartesian strains

$$\begin{aligned} E_{me}|_{\text{cubic}} = & \sum_l \left[\left(B^{a,l} S^{a,l} + B^{\gamma,l} \left(-\frac{1}{2} S_1^\gamma + \frac{\sqrt{3}}{2} S_2^\gamma \right) \right) \epsilon_{xx} \right. \\ & + \left(B^{a,l} S^{a,l} + B^{\gamma,l} \left(-\frac{1}{2} S_1^\gamma - \frac{\sqrt{3}}{2} S_2^\gamma \right) \right) \epsilon_{yy} \\ & \left. + (B^{a,l} S^{a,l} + B^{\gamma,l} S_1^\gamma) \epsilon_{zz} + B^{e,l} (S_1^{e,l} \epsilon_{yz} + S_2^{e,l} \epsilon_{zx} + S_3^{e,l} \epsilon_{xy}) \right] \quad (2.7a) \end{aligned}$$

$$\begin{aligned} E_{me}|_{\text{hex}} = & \sum_l [B^{a1,l} (\epsilon_{xx} + \epsilon_{yy} + \epsilon_{zz}) S^{a1,l} + B^{a2,l} (2\epsilon_{zz} - \epsilon_{xx} - \epsilon_{yy}) S^{a2,l} \\ & + B^{\gamma,l} ((\epsilon_{xx} - \epsilon_{yy}) S_1^{\gamma,l} + \epsilon_{xy} S_2^{\gamma,l}) + B^{e,l} (\epsilon_{zx} S_1^{e,l} + \epsilon_{yz} S_2^{e,l})]. \quad (2.7b) \end{aligned}$$

Or for $l = 0, 2$

$$\begin{aligned} E_{me}|_{\text{cubic}} = & b_0(\epsilon_{xx} + \epsilon_{yy} + \epsilon_{zz}) + b_1(\alpha_x^2 \epsilon_{xx} + \alpha_y^2 \epsilon_{yy} + \alpha_z^2 \epsilon_{zz}) \\ & + b_2(\alpha_x \alpha_y \epsilon_{xy} + \alpha_y \alpha_z \epsilon_{yz} + \alpha_z \alpha_x \epsilon_{zx}) \quad (2.8a) \end{aligned}$$

$$\begin{aligned} E_{me}|_{\text{hex}} = & b_{11}(\epsilon_{xx} + \epsilon_{yy}) + b_{12} \epsilon_{zz} + b_{21}(\alpha_z^2 - \frac{1}{3})(\epsilon_{xx} + \epsilon_{yy}) + b_{22}(\alpha_z - \frac{1}{3}) \epsilon_{zz} \\ & + b_3(\alpha_x^2 - \alpha_y^2)(\epsilon_{xx} - \epsilon_{yy}) + \alpha_x \alpha_y \epsilon_{xy} + b_4(\alpha_z \alpha_x \epsilon_{zx} + \alpha_y \alpha_z \epsilon_{yz}). \quad (2.8b) \end{aligned}$$

The relationships between the conventional magnetoelastic constants (Kittel 1949) and the symmetry constants are given in table 3.

In a similar fashion, the elastic energy, E_{el} , takes the following form in terms

of symmetry strains

$$E_{el}|_{\text{cubic}} = \frac{1}{2}C^\alpha(\epsilon^\alpha)^2 + \frac{1}{2}C^\gamma((\epsilon_1^\gamma)^2 + (\epsilon_2^\gamma)^2) + \frac{1}{2}C^\epsilon((\epsilon_1^\epsilon)^2 + (\epsilon_2^\epsilon)^2 + (\epsilon_3^\epsilon)^2) \quad (2.9a)$$

$$\begin{aligned} E_{el}|_{\text{hex}} = & \frac{1}{2}C_{11}^\alpha(\epsilon^\alpha)^2 + C_{12}^\alpha(\epsilon^\alpha)(\epsilon^\alpha) + \frac{1}{2}C_{22}^\alpha(\epsilon^\alpha)^2 \\ & + \frac{1}{2}C^\gamma((\epsilon_1^\gamma)^2 + (\epsilon_2^\gamma)^2) + \frac{1}{2}C^\epsilon((\epsilon_1^\epsilon)^2 + (\epsilon_2^\epsilon)^2). \end{aligned} \quad (2.9b)$$

Transforming to the cartesian strains

$$\begin{aligned} E_{el}|_{\text{cubic}} = & \frac{1}{2}C_{11}(\epsilon_{xx}^2 + \epsilon_{yy}^2 + \epsilon_{zz}^2) + C_{12}(\epsilon_{yy}\epsilon_{zz} + \epsilon_{zz}\epsilon_{xx} + \epsilon_{xx}\epsilon_{yy}) \\ & + \frac{1}{2}C_{44}(\epsilon_{xy}^2 + \epsilon_{yz}^2 + \epsilon_{zx}^2) \end{aligned} \quad (2.10a)$$

$$\begin{aligned} E_{el}|_{\text{hex}} = & \frac{1}{2}C_{11}(\epsilon_{xx}^2 + \epsilon_{yy}^2) + C_{12}\epsilon_{xx}\epsilon_{yy} + \frac{1}{2}C_{33}\epsilon_{zz}^2 + C_{13}(\epsilon_{xx}\epsilon_{zz} + \epsilon_{yy}\epsilon_{zz}) \\ & + \frac{1}{2}C_{44}(\epsilon_{yz}^2 + \epsilon_{zx}^2) + \frac{1}{4}(C_{11} - C_{12})\epsilon_{xy}^2. \end{aligned} \quad (2.10b)$$

The relationships between the symmetry constants and the conventional elastic constants are given in table 3.

The magnetostriction, $\Delta l/l$, is determined in the conventional way from the definition (Kittel 1949)

$$\Delta l/l = \sum_{i>j} \epsilon_{ij}^{eq} \beta_i \beta_j \quad (2.11)$$

where the ϵ_{ij}^{eq} are the equilibrium strains determined from

$$\delta E / \delta \epsilon_{ij} = 0. \quad (2.12)$$

For the cubic case

$$\begin{aligned} \epsilon_{ii}^{eq} &= -b_1 \alpha_i^2 / (c_{11} - c_{12}) - b_0 / (c_{11} + 2c_{12}) + c_{12} b_1 / (c_{11} + 2c_{12})(c_{11} - c_{12}) \\ \epsilon_{ij}^{eq} &= -b_2 \alpha_i \alpha_j / c_{44}. \end{aligned} \quad (2.13a)$$

TABLE 3
Relation between symmetry and cartesian
elastic constants and magnetoelastic con-
stants

Cubic	Hexagonal
$c_{11} = C^\alpha + C^\gamma$	$c_{11} = C_{11}^\alpha - C_{12}^\alpha + \frac{1}{4}C_{22}^\alpha + C^\gamma$
$c_{12} = C^\alpha - \frac{1}{2}C^\gamma$	$c_{12} = C_{11}^\alpha - C_{12}^\alpha + \frac{1}{4}C_{22}^\alpha - C^\gamma$
$c_{44} = C^\epsilon$	$c_{33} = C_{11}^\alpha + 2C_{12}^\alpha + C_{22}^\alpha$
	$c_{13} = C_{11}^\alpha + \frac{1}{2}C_{12}^\alpha - \frac{1}{2}C_{22}^\alpha$
	$c_{44} = C^\epsilon$
$b_0 = B^\alpha - \frac{1}{2}B^\gamma$	$b_{11} = B^{\alpha+1,0} - B^{\alpha+2,0}$
$b_1 = \frac{1}{2}B^\gamma$	$b_{12} = B^{\alpha+1,0} + 2B^{\alpha+2,0}$
$b_2 = B^{\epsilon+2}$	$b_{21} = B^{\alpha+1,2} - B^{\alpha+2,2}$
	$b_{22} = B^{\alpha+2,2} + 2B^{\alpha+2,2}$
	$b_3 = B^{\gamma+2}$
	$b_4 = B^{\epsilon+2}$

For the hexagonal case

$$\begin{aligned}\epsilon_{xx}^{eq} &= \frac{-b_{11}c_{33} + b_{12}c_{13}}{D} + \frac{(-b_{12}c_{33} + b_{22}c_{13})(\alpha_x^2 - \frac{1}{3})}{D} - \frac{b_3(\alpha_x^2 - \alpha_y^2)}{2(c_{11} - c_{12})} \\ \epsilon_{yy}^{eq} &= \frac{-b_{11}c_{33} + b_{12}c_{13}}{D} + \frac{(-b_{12}c_{33} + b_{22}c_{13})(\alpha_z^2 - \frac{1}{3})}{D} + \frac{b_3(\alpha_x^2 - \alpha_y^2)}{2(c_{11} - c_{12})} \\ \epsilon_{zz}^{eq} &= \frac{2c_{13}b_{11} - (c_{11} + c_{12})b_{12}}{D} + \frac{(2c_{13}b_{21} - (c_{11} + c_{12})b_{22})(\alpha_z^2 - \frac{1}{3})}{D} \\ \epsilon_{xy}^{eq} &= \frac{-b_3\alpha_x\alpha_y}{\frac{1}{2}(c_{11} - c_{12})} \quad \epsilon_{yz}^{eq} = \frac{-b_4\alpha_y\alpha_z}{c_{44}} \quad \epsilon_{zx}^{eq} = \frac{-b_4\alpha_z\alpha_x}{c_{44}}\end{aligned}\quad (2.13b)$$

where $D = c_{33}(c_{11} + c_{12}) - 2c_{13}^2$.

Substituting these expressions into eq. (2.11), we find to second degree in α_i

$$\begin{aligned}\Delta l/l|_{cubic} &= \lambda^\alpha + \frac{1}{2}\lambda_{100}(\alpha_x^2\beta_x^2 + \alpha_y^2\beta_y^2 + \alpha_z^2\beta_z^2 - \frac{1}{3}) \\ &\quad + 3\lambda_{111}(\alpha_x\alpha_y\beta_x\beta_y + \alpha_y\alpha_z\beta_y\beta_z + \alpha_z\alpha_x\beta_z\beta_x)\end{aligned}\quad (2.14a)$$

where

$$\begin{aligned}\lambda^\alpha &= -3b_0/(c_{11} + c_{12}) + 3c_{12}b_1/(c_{11} + 2c_{12})(c_{11} - c_{12}) \\ \lambda_{100} &= -2b_1/3(c_{11} - c_{12}) \\ \lambda_{111} &= -b_2/3c_{44}\end{aligned}$$

and

$$\begin{aligned}\Delta l/l|_{hex} &= \lambda^{\alpha 1.0}(\beta_x^2 + \beta_y^2) + \lambda^{\alpha 2.0}\beta_z^2 \\ &\quad + \lambda^{\alpha 1.2}(\alpha_x^2 - \frac{1}{3})(\beta_x^2 + \beta_y^2) + \lambda^{\alpha 2.2}(\alpha_z^2 - \frac{1}{3})\beta_z^2 \\ &\quad + \lambda^{\gamma 2}[\frac{1}{2}(\alpha_x^2 - \alpha_y^2)(\beta_x^2 - \beta_y^2) + 2\alpha_x\alpha_y\beta_x\beta_y] \\ &\quad + 2\lambda^{\epsilon 2}[\alpha_y\alpha_z\beta_y\beta_z + \alpha_z\alpha_x\beta_z\beta_x]\end{aligned}\quad (2.14b)$$

where

$$\begin{aligned}\lambda^{\alpha 1.0} &= (b_{11}c_{33} + b_{12}c_{13})/D \\ \lambda^{\alpha 2.0} &= (2b_{11}c_{13} - b_{12}(c_{11} + c_{12}))/D \\ \lambda^{\alpha 1.2} &= (-b_{21}c_{33} + b_{22}c_{13})/D \\ \lambda^{\alpha 2.2} &= (2b_{21}c_{13} - b_{22}(c_{11} + c_{12}))/D \\ \lambda^{\gamma 2} &= -b_3/(c_{11} - c_{12}) \\ \lambda^{\epsilon 2} &= -b_4/2c_{44}.\end{aligned}$$

The symmetry modes are depicted in fig. 1. Expressions for the magnetostriction up to α_6^6 are given in Appendix A.

When the crystals are free to strain under magnetization rotation (constant external stress), the presence of magnetoelasticity gives rise to a contribution to the anisotropy not included in E_a . (For a clamped lattice, there is no magnetostrictive contribution to the anisotropy.) For a cubic system, the magnetostriction affects the lowest order anisotropy expression. Substituting ϵ_u^{eq} and

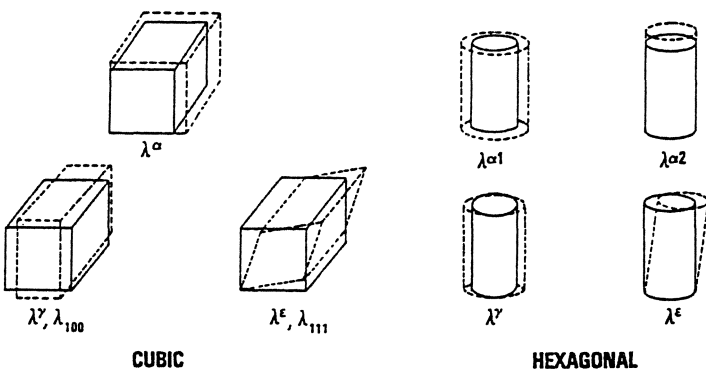


Fig. 1. Magnetostriiction modes for cubic and hexagonal symmetries.

ϵ_{ij}^{eq} from eq. (2.13a) into eqs. (2.8a) and (2.10a), the total energy at constant stress (σ) becomes

$$E^\sigma = E_0 + K_1'(\alpha_x^2\alpha_y^2 + \alpha_y^2\alpha_z^2 + \alpha_z^2\alpha_x^2) \quad (2.15)$$

where

$$K_1' = K_1 + b_1^2/(c_{11} - c_{12}) - b_2^2/2c_{44}.$$

In the hexagonal system, the lowest order anisotropy constant is not affected by the magnetostriiction.

3. Magnetostriiction of binary rare earth-iron alloys

The heavy rare earth elements, Tb and Dy, display the largest known magnetostrictions (Rhyne and Legvold 1965, Clark et al. 1965). Below their ordering temperatures, the magnetically induced strains overwhelm the conventional thermal expansion of the crystal axes (fig. 2). These large magnetostrictions are a direct consequence of the huge strain dependence of the magnetic anisotropy. In the heavy rare earth metals, J is a good quantum number, and for Tb and Dy, the intrinsic magnetostrictions ($\lambda^{\gamma^2}(0\text{ K})$) are almost identical to each other, in agreement with Stevens' equivalent operator calculations (Tsuya et al. 1964). The magnetostriiction and anisotropy of the rare earths, however, are huge *only* at cryogenic temperatures. All of the magnetostriuctive rare earths possess ordering temperatures below room temperature. Because of this, only a small paramagnetic magnetostriiction ($\lambda \propto H^2$) exists at room temperature, even for Tb and Dy.

To achieve highly magnetostriuctive materials at room temperature, alloys of the type R_xT_{1-x} , where $R = \text{Sm, Tb, Dy, Ho, Er, Tm}$, and $T = \text{Ni, Co and Fe}$, were investigated. The addition of Ni, Co and Fe to the rare earths produces compounds and amorphous alloys which in some cases have higher Curie temperatures than the elements, and in others, much lower ones (see Taylor

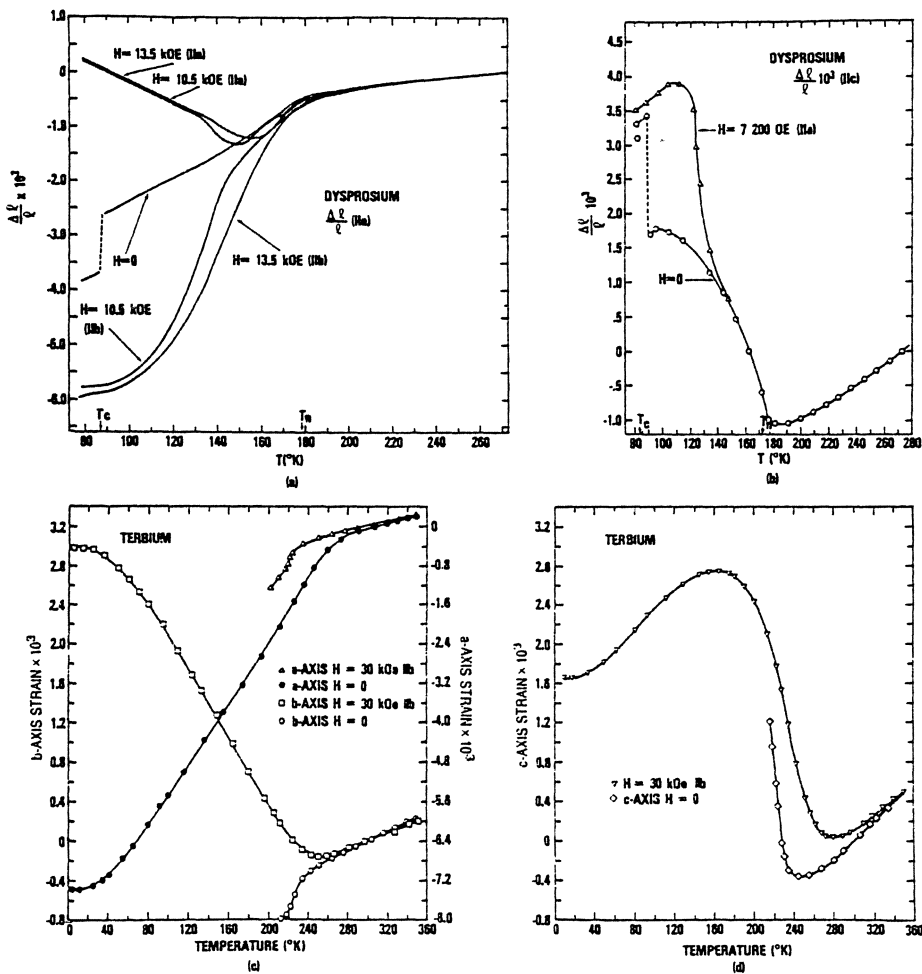


Fig. 2. Magnetostriiction of dysprosium and terbium single crystals (Dy, taken from Clark et al. 1965; Tb, taken from Rhyne and Legvold 1965).

1971, Rhyne 1978). In fact, all the Ni compounds have Curie temperatures below 200 K. The Curie temperatures of the Co compounds span a wide range from the high T_C of 1200 K for Tb_2Co_{17} to near 0 K for Er_3Co . The R_xFe_{1-x} compounds have an anomalous Curie temperature dependence on composition x , in which the most Fe rich compound (R_2Fe_{17}) possesses the lowest T_C and the least iron rich (RFe_2) possesses the highest. Amorphous rare earth transition metal alloys produced both by rapid sputtering and evaporation techniques also possess a wide range of ordering temperatures, some of which are higher than their crystalline counterparts (most Co alloys) and some of which are lower (most Fe

alloys). In view of this, the R_xT_{1-x} alloys with the greatest potential to achieve large room temperature magnetostrictions are the cubic Laves phase RFe_2 compounds with $R = Tb$ and Dy.

The first compound observed to exhibit a large magnetostriction ($\sim 2 \times 10^{-3}$) at room temperature was $TbFe_2$ (Clark and Belson 1972). This compound possesses the largest room temperature magnetostriction known to date. In table 4 are gathered the room temperature magnetostrictions of some typical ferro- and

TABLE 4
Magnetostriction of some polycrystalline materials at room temperature*

Material	$10^6\lambda_s$	Reference	Material	$10^6\lambda_s$	Reference
Ni	-33	a	$TbFe_2$	1753	h
Co	-62	b	$TbNi_{0.4}Fe_{1.6}$	1151	k
Fe	-9	c	$TbCo_{0.4}Fe_{1.6}$	1487	k
60% Co 40% Fe	68	d	$TbFe_2$ (amorphous)	308	h
60% Ni 40% Fe	25	e	$DyFe_2$	433	h
$NiFe_2O_4$	-26	f	$DyFe_2$ (amorphous)	38	k
$Co_2Fe_2O_4$	-110	f	$HoFe_2$	80	l
Fe_3O_4	40	f	$ErFe_2$	-299	h
$Y_3Fe_5O_12$	-2	g	$TmFe_2$	-123	h
Tb_2Ni_{17}	-4	h	$SmFe_3$	-211	m
YCo_3	0.4	h	$TbFe_3$	693	m
$TbCo_3$	65	h	$DyFe_3$	352	m
Y_2Co_{17}	80	i	$HoFe_3$	57	m
Pr_2Co_{17}	336	i	$ErFe_3$	-69	m
Tb_2Co_{17}	207	i	$TmFe_3$	-43	m
Dy_2Co_{17}	73	i	Ho_2Fe_{23}	58	m
Er_2Co_{17}	28	i	Er_6Fe_{23}	-36	m
$Tb_{0.04}(Co_{0.5}Fe_{0.5})$	95	j	Tm_6Fe_{23}	-25	m
85 Wt % Tb }			Sm_2Fe_{17}	-63	m
15 Wt % Fe }	539	h	Tb_2Fe_{17} (as cast)	131	m
70 Wt % Tb }			Tb_2Fe_{17}	-14	m
30 Wt % Fe }	1590	h	Dy_2Fe_{17}	-60	m
YFe_2	1.7	h	Ho_2Fe_{17}	-106	m
$SmFe_2$	-1560	h	Er_2Fe_{17}	-55	m
$GdFe_2$	39	m	Tm_2Fe_{17}	-29	m

* For the rare earth compounds, λ_s denotes $\frac{1}{2}(\lambda_l - \lambda_\perp)$ at some large field (see references below).

^a Went (1951).

^b A.E. Miller, unpublished. Here λ_s denotes

^b Yamamoto and Miyasawa (1965).

^b $\frac{1}{2}(\lambda_l - \lambda_\perp)$ at 14 kOe.

^c Weil and Reichel (1954).

^b Sato et al. (1976).

^d S.R. Williams (1932).

^b A.E. Clark and R. Abbundi, unpublished.

^e Masiyama (1931).

^b Koon et al. (1974).

^f See: Ferrites by Smit and Wijn (1959).

^m Abbundi and Clark (1978). Also Naval Sur-

^g Clark et al. (1963b).

face Weapons Center TR78-88, Dahlgren.

^h Clark (1974). Here λ_s denotes $\frac{1}{2}(\lambda_l - \lambda_\perp)$ at 25 kOe.

^{V.A.} λ_s denotes $\frac{1}{2}(\lambda_l - \lambda_\perp)$ at 25 kOe.

ferrimagnets, some rare earth-cobalt compounds and some rare earth-iron compounds. While the RFe₂ compounds TbFe₂ and SmFe₂ possess the largest room temperature magnetostrictions, large magnetostrictions are also found in some RFe₃, and R₂Co₁₇ compounds. Contrary to expectations, DyFe₂ possesses a much smaller magnetostriction than TbFe₂.

In figs. 3, 4, 5 and 6 the magnetostrictions of the rare earth-iron compounds are plotted vs. applied field. Here $\lambda_{\parallel} - \lambda_{\perp}$ denotes the fractional change in length as an applied field is rotated from perpendicular to parallel to the measurement direction. For isotropic polycrystals $\lambda_{\parallel} - \lambda_{\perp} = \frac{1}{2}\lambda_s$.

TbFe₂ and SmFe₂ possess the largest strains by far and are the basis of the multicomponent systems of sections 6, 7, and 8. For SmFe₂, $\lambda_{\parallel} - \lambda_{\perp} < -2000 \times 10^{-6}$; for TbFe₂, $\lambda_{\parallel} - \lambda_{\perp} > 2000 \times 10^{-6}$. In both of these compounds the rare earth ion is highly anisotropic (Sm - most prolate in form; Tb - most oblate in form) and the rare earth-iron exchange is large, which keeps the rare earth sublattice magnetization nearly intact at room temperature. Thus the large magnetostriction does not fall appreciably from its low temperature value. Unlike the elements, where the magnetostriction of Tb and Dy are similar, the magnetostriction of DyFe₂ is much smaller than that of TbFe₂ and exhibits a

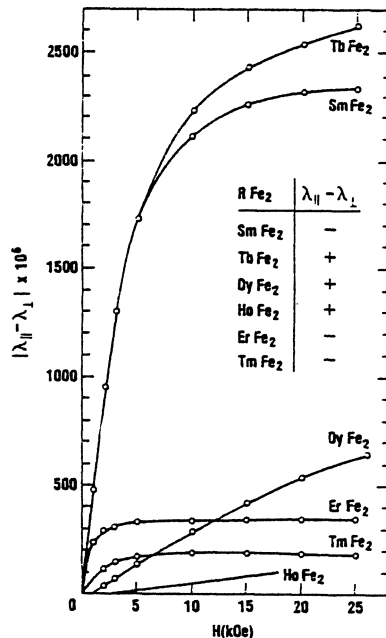


Fig. 3. Room temperature magnetostriction of rare earth-Fe₂ polycrystals (SmFe₂, TbFe₂, DyFe₂, ErFe₂ and TmFe₂ taken from Clark 1974; HoFe₂ taken from Koon et al. 1974).

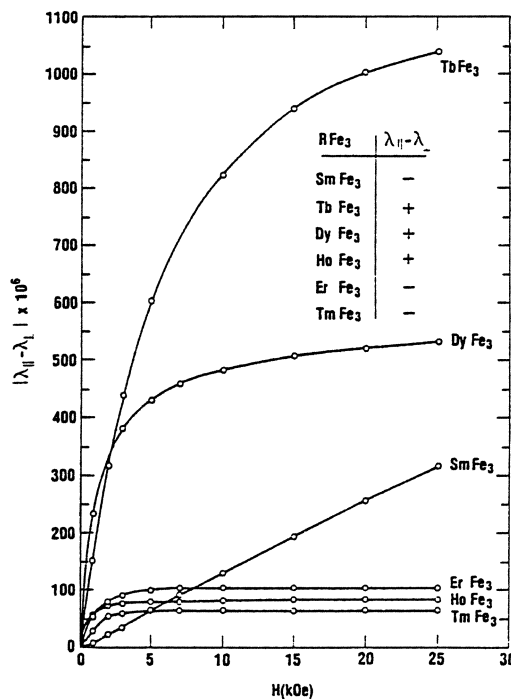


Fig. 4. Room temperature magnetostriction of rare earth-Fe₃ polycrystals (taken from Abbundi and Clark 1978).

slow increase with magnetic field (fig. 3). This is indicative of a very large magnetocrystalline anisotropy. As will be shown in section 5, the anisotropy is indeed large at room temperature. While the magnetostrictions of DyFe₂ and HoFe₂ are far from saturation at room temperature with laboratory fields, the magnetostrictions of the remaining RFe₂ compounds display rather well defined knees. In the compounds SmFe₂, TbFe₂, ErFe₂ and TmFe₂, the magnetization lies along the [111] whereas for the DyFe₂ and HoFe₂ compounds, it lies parallel to [100] (see section 4). Because of this, the absence of a large magnetostriction at low fields for DyFe₂ and HoFe₂ leads to the conjecture that $\lambda_{111} \gg \lambda_{100}$ at room temperature (Clark 1974). The increasing magnetostriction with increasing field in the case of polycrystalline DyFe₂ and HoFe₂ is attributed to the sensing of a large λ_{111} as the magnetic moments in the crystallites are rotated away from their easy [100] axes. The magnetostriction of the Sm, Tb, Er and Tm compounds is large at low fields, directly reflecting the large λ_{111} . Similar field dependences were found below room temperature in polycrystalline TbFe₂ and DyFe₂ (Clark and Belson 1972) and in polycrystalline DyFe₂, HoFe₂ and ErFe₂ (Koon et al. 1971).

In fig. 7, the effect of replacing Fe by Co in TbFe₂ is illustrated. Since the Curie temperature does not fall appreciably in TbFe_{2(1-x)}Co_{2x} for $x < 0.5$, the

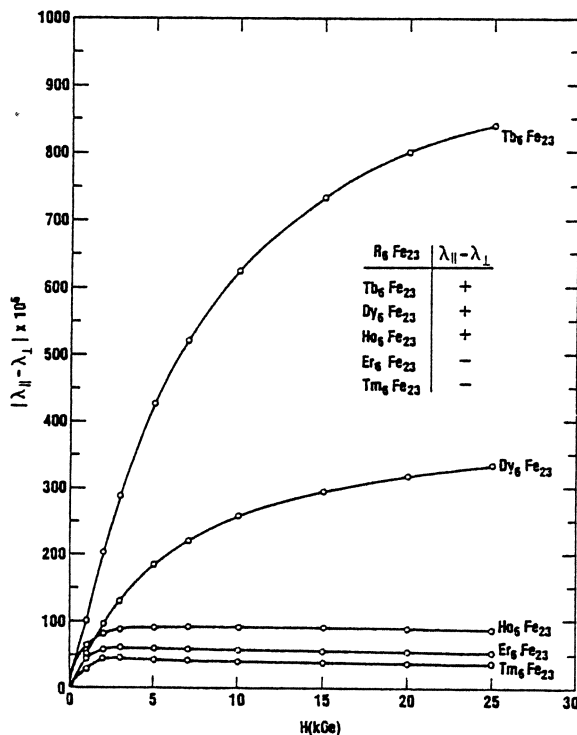


Fig. 5. Room temperature magnetostriction of R_6Fe_{23} polycrystals (taken from Abbundi and Clark 1978). Tb₆Fe₂₃ and Dy₆Fe₂₃ are not completely single phase.

relative magnetostriction, as measured by the distortion of the cubic cell (Dwight and Kimball 1974) remains almost constant over this concentration range. Strain gage measurements by Belov et al. (1975) show a more rapid decrease in magnetostriction with increasing Co concentration. This may be due to preferred orientation of their polycrystalline samples.

Single crystals of TbFe₂, DyFe₂, HoFe₂, ErFe₂ and TmFe₂ have been prepared by Bridgman, Czochralski and induction zoning methods (McMasters, unpublished, 1978, Williams and Koon 1975, Milstein 1976). In fig. 8, values of λ_{111} are shown for TbFe₂, ErFe₂ and TmFe₂ at room temperature. In these crystals [111] is the easy magnetization direction. The compounds DyFe₂ and HoFe₂, on the other hand, possess [100] as the easy magnetization axis. In these materials therefore λ_{100} , rather than λ_{111} , is sensed at technical saturation. Room temperature field dependences of λ_{100} are shown in fig. 9. In remarkable contrast to the large values of λ_{111} for TbFe₂ and ErFe₂, for DyFe₂, $\lambda_{100} = 4 \times 10^{-6}$ and for HoFe₂, $\lambda_{100} = -59$ to -66×10^{-6} (Clark et al. 1976, Koon, unpublished, Abbundi et al. 1979). Such a highly anisotropic magnetostriction ratio, $|\lambda_{111}/\lambda_{100}| \gg 1$, is uncommon. It reveals the immense importance of grain orientation in achieving high magnetostriction in

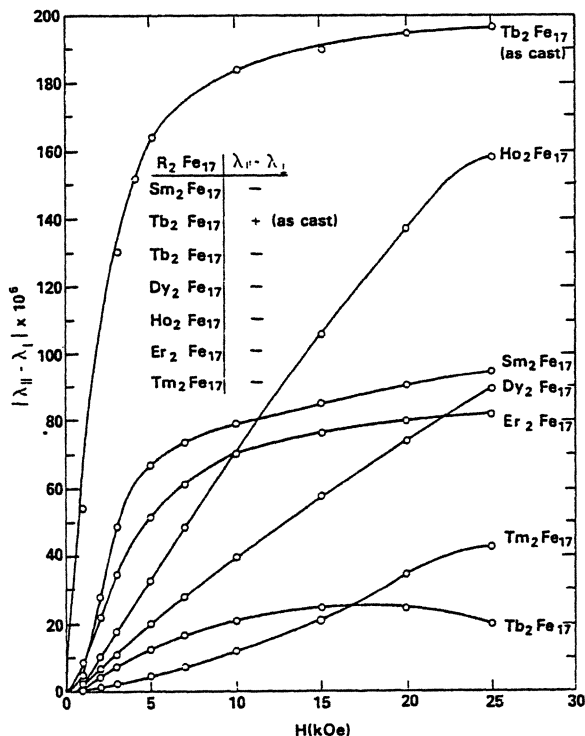


Fig. 6. Room temperature magnetostriction of R_2Fe_{17} polycrystals (taken from Abbundi and Clark 1978). Tb_2Fe_{17} and Dy_2Fe_{17} contain both rhombohedral and hexagonal phases. With the exception of Tb_2Fe_{17} (as cast), all samples were heat treated at 1000°C.

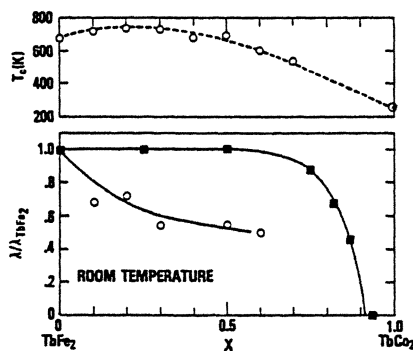


Fig. 7. Curie temperature and relative magnetostriiction of $TbFe_{2(1-x)}Co_{2x}$ (taken from ■ Dwight and Kimball 1974, and ○ Belov et al. 1975).

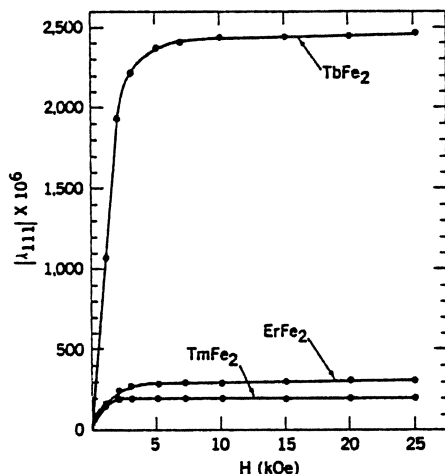


Fig. 8. Room temperature magnetostriction $|\lambda_{111}|$ for single crystal TbFe₂, ErFe₂ and TmFe₂ (taken from Clark et al. 1975, Abbundi and Clark 1978). For TbFe₂, $\lambda_{111} > 0$; for ErFe₂ and TmFe₂, $\lambda_{111} < 0$.

polycrystal $R\text{Fe}_2$ materials. In an optimally oriented polycrystal, $\lambda_s \approx \lambda_{111}$; in an isotropic polycrystal, $\lambda_s \approx 0.6\lambda_{111}$; and in a poorly textured polycrystal, $\lambda_s \approx 0$. The effect of crystallite orientation can be two-fold beneficial. In addition to the increase in magnetostriction constant, λ_s , a preferentially oriented polycrystal possesses the major advantage of far lower internal losses at grain boundaries. This is important in applications where a high magnetostriction at low applied fields is required.

In fig. 10, $\lambda_{111}(T)$ of TbFe₂ and $\lambda_{100}(T)$ of DyFe₂ are contrasted (Clark et al.

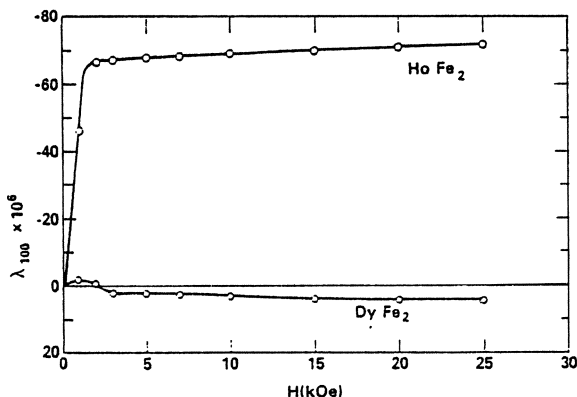


Fig. 9. Room temperature magnetostriiction (λ_{100}) for single crystal DyFe₂ and HoFe₂ (taken from Abbundi, Clark and Koon, unpublished).

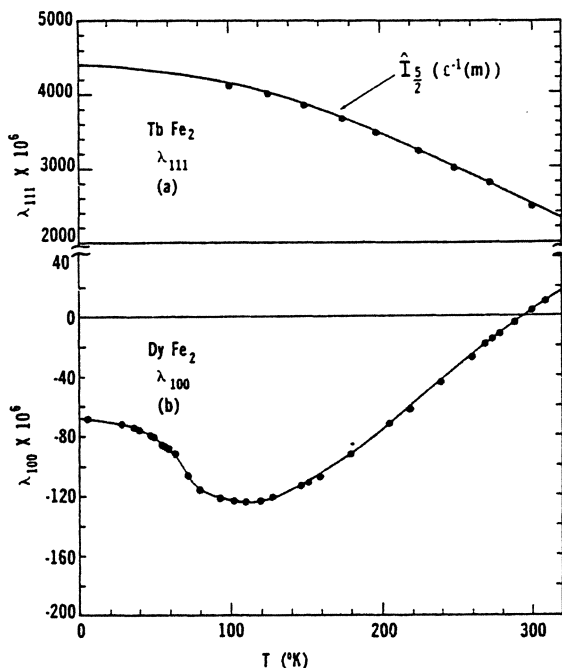


Fig. 10. Temperature dependence of the magnetostriction for single crystal TbFe_2 and DyFe_2 (taken from Clark et al. 1977).

1977). $\lambda_{111}(T)$ is well behaved. The magnetostriction monotonically decreases with increasing temperature according to the single-ion temperature dependence (Callen and Callen 1963) (see section 4). At absolute zero, $\lambda_{111}(0) = 4400 \times 10^{-6}$ for TbFe_2 the largest known value for a cubic material. On the other hand, $\lambda_{100}(T)$ is small for DyFe_2 and cannot be fit by a simple single-ion function. This is also true for HoFe_2 where $|\lambda_{100}|$ is much larger [$\lambda_{100}(0) = -7.45 \times 10^6$]. See Abbundi et al. (1979).

TmFe_2 possesses a comparatively small magnetostriction at room temperature. This, however, reflects the weak Tm-Fe exchange and low room temperature Tm magnetization, rather than a small intrinsic magnetoelastic coupling. In fig. 11, the rapid rise of $|\lambda_{111}|$ with decreasing temperature to a value approaching that of TbFe_2 at 4 K is illustrated. A fit to the data with single-ion theory (section 4) is excellent. Over this range, the magnetostriction changes by a factor of 15. The dip in the observed magnetostriction of TmFe_2 at 235 K is a consequence of the cancellation of sublattice magnetizations at its compensation temperature, where the moments lie perpendicular to the applied field direction. The forced magnetostriction is observed to change sign at this temperature as the Tm moment rotates from parallel to the applied field direction for $T < T_{\text{comp}}$ to antiparallel to the applied field direction for $T > T_{\text{comp}}$.

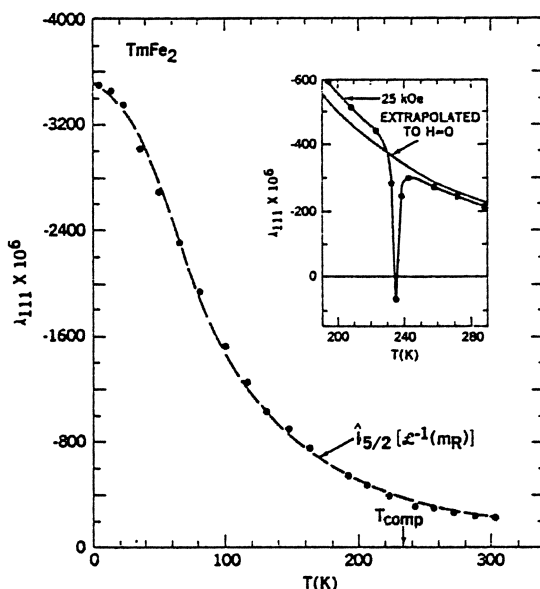


Fig. 11. Magnetostriiction (λ_{111}) of single crystal TmFe_2 (taken from Abbundi and Clark 1978).

A large magnetoelastic coupling, b_2 , is also inferred for SmFe_2 . No single crystal measurements have yet been reported. In fig. 12 the magnetostriiction of polycrystal SmFe_2 , taken from Rosen et al. (1974), is plotted as a function of temperature. The magnetoelastic coupling indeed is high. However, an analysis of the temperature dependence is difficult because of a low lying $J = \frac{7}{2}$ multiplet. A

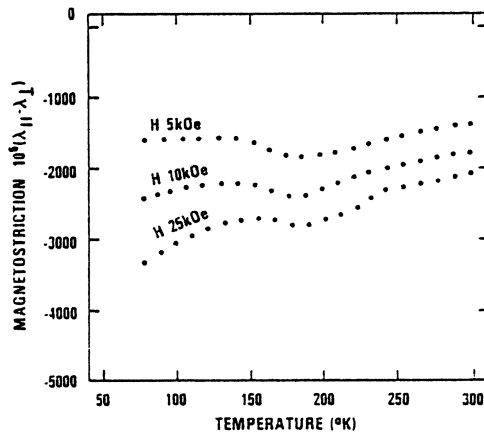


Fig. 12. Magnetostriiction of SmFe_2 (taken from Rosen et al. 1974).

broad peak in $|\lambda_{\parallel} - \lambda_{\perp}|$ is observed between 140 K and 240 K where the easy axis of magnetization rotates from [110] to [111] with increasing temperature.

An atomic model for the anisotropic magnetostriction based upon the structure of the cubic Laves phase C15 compounds was proposed by Clark et al. (1976) and Cullen and Clark (1977). In this model, potentially huge values of λ_{100} , arising from the asymmetry of the rare earth 4f electron shell, are effectively shorted out because of the high tetrahedral ($\bar{4}3m$) symmetry at the rare earth sites. On the other hand, huge λ_{111} 's are allowed because two inequivalent tetrahedral sites exist in the C15 structure which permit internal distortions along [111] directions. *This internal distortion lowers the symmetry and drives an external rhombohedral distortion (λ_{111})*. In fig. 13, the distortion is illustrated for $TbFe_2$ and other RFe_2 compounds containing rare earths with oblate 4f charge distributions. The two inequivalent sites, situated at 0, 0, 0 and $\frac{1}{4}, \frac{1}{4}, \frac{1}{4}$ are denoted by A (or A') and B (or B') respectively. The iron atoms are not shown. λ_{111} signifies the fractional change in length along the [111] direction when the material is magnetized along this direction. In fig. 13a, the magnetization is directed along [111]. The oblate 4f electron cloud ($-e$) lies perpendicular to the magnetization axis. Considering only the electrostatic coulomb interaction, the closer proximity of the 4f electron cloud on A to atoms B', than to atom B, causes an extension of the A-B bond, the magnitude of which depends upon the internal A-B modulus. The resultant increase in a exceeds a small decrease in b , yielding a net positive external magnetostriction along [111]. Conversely, for compounds with rare earths possessing prolate 4f charge densities, e.g. for $SmFe_2$, $ErFe_2$ and $TmFe_2$, a contraction of a occurs, producing the observed negative magnetostrictions (λ_{111}). A large rhombohedral distortion thus exists

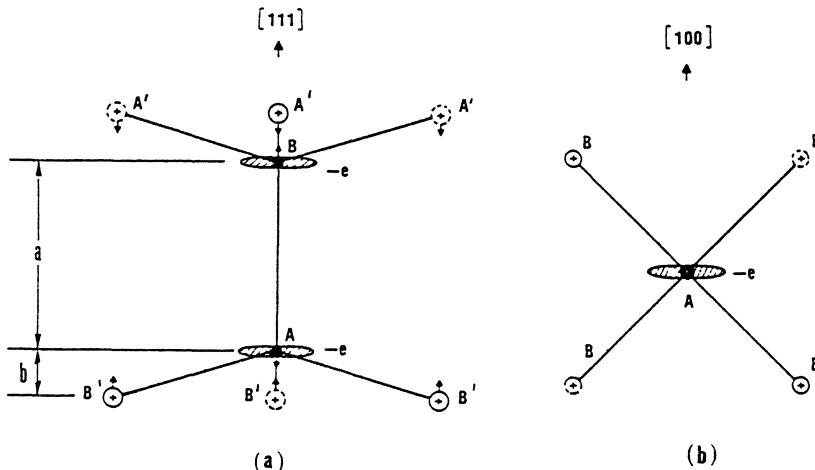


Fig. 13. Model of magnetostriction in Laves phase RFe_2 compounds: (a) $M \parallel [111]$, (b) $M \parallel [100]$. Open circles, O, denote atoms above plane of figure; broken circles, \circlearrowleft , denote atoms below (taken from Clark et al. 1976).

whenever the magnetization points along [111], i.e. for TbFe₂, SmFe₂, ErFe₂ and TmFe₂. The alternate case of [100] easy, i.e. for DyFe₂ and HoFe₂, is depicted in fig. 13b. With the easy direction of magnetization parallel to the [100] direction, the 4f electron cloud becomes equidistant to all rare earth nearest neighbors, allowing no magnetostrictively driven internal distortion via point charge electrostatic interactions. All A-B bonds are equivalent, the symmetry remains high, and the potentially huge magnetostriction constant, λ_{100} , does not appear. To date these internal distortions have not yet been verified.

Of the total of fifteen lanthanide rare earths, only a few form highly magnetostrictive RFe₂ compounds at room temperature. In table 5 are listed the rare earth elements in order of the increasing number of 4f electrons. La with no 4f electrons and Lu with a full shell of fourteen 4f electrons are omitted. It is possible to calculate the intrinsic ($T = 0$ K) magnetostrictive contribution of each 3⁺ rare earth ion for a particular compound (assuming its existence) given the magnetostriction of at least one compound (e.g. TbFe₂). The theory utilizes the Stevens' equivalent operator method. According to Stevens (1952), the ratio of the intrinsic magnetostriction of one rare earth to another is given by the ratio of $\alpha J (J - \frac{1}{2}) \langle r_f^2 \rangle$ where α is the lowest order Stevens' factor, J is the ground state angular momentum for the 3⁺ ion and $\langle r_f^2 \rangle$ is the average radius squared of the 4f electron shell. Here the effect of screening (Freeman and Watson 1962) is neglected. In table 5, the values of J , α , and $\langle r_f^2 \rangle$ are given along with the calculated values of λ_{111} for RFe₂ compounds, normalized to 4400×10^{-6} for TbFe₂. The estimated uncertainty

TABLE 5
Magnetostriction of RFe₂ compounds

R	$\alpha \times 10^{2a}$	J	$\langle r_f^2 \rangle^b$	$\lambda_{111} \times 10^6(\text{calc})^*$	$\lambda_{111} \times 10^6(\text{exp})$
				0 K	room temperature
Ce*	-5.72	$\frac{5}{2}$	1.20	6000	-
Pr*	-2.10	4	1.086	5600	-
Nd*	-0.643	$\frac{9}{2}$	1.001	2000	-
Pm*	0.772	4	0.942	-1800	-
Sm	4.13	$\frac{5}{2}$	0.883	-3200	-2100 ^c
Eu*	0	0	0.834	0	-
Gd	0	$\frac{7}{2}$	0.785	0	-
Tb	-1.01	6	0.756	4400	2460 ^d
Dy	-0.635	$\frac{15}{2}$	0.726	4200	1260 ^d
Ho	-0.222	8	0.696	1600	185 ^e , 200 ^f
Er	-0.254	$\frac{15}{2}$	0.666	-1500	-300 ^d
Tm	1.01	6	0.639	-3700	-210 ^d
Yb*	3.18	$\frac{7}{2}$	0.613	-3600	-

* Calculated for cubic Laves phase R³⁺Fe₂ compounds. For R = Ce, Nd, Pm, Eu and Yb, this compound has not yet been synthesized. PrFe₂ has been synthesized only under high pressure.

^a Stevens (1952).

^c Clark et al. (1976).

^b Freeman and Watson (1962).

^d Abbundi and Clark (1978).

^e Koon and Williams (1977).

^f Abbundi et al. (1979).

^g Clark et al. (1975).

in the absolute magnitude of $\lambda_{111}(0)$ is $\pm 15\%$. Note that the largest positive intrinsic magnetostrictions are those calculated for CeFe₂, PrFe₂, TbFe₂, and DyFe₂; the largest negative magnetostrictions are those calculated for SmFe₂, TmFe₂ and YbFe₂. However, not all of these compounds have been synthesized. Ce and Yb are not found in their trivalent states. The calculated magnetostrictions of quadrivalent Ce and divalent Yb are zero. PrFe₂ and NdFe₂ do not readily form the cubic Laves phase compounds. While both DyFe₂ and TmFe₂ have high incipient magnetostrictions, the large magnetostriction is not realized in DyFe₂ since [111] is magnetically hard, and the large magnetostriction of TmFe₂ is realized only at low temperatures because of a weak thulium-iron exchange interaction. Thus only TbFe₂ and SmFe₂ emerge with large room temperature magnetostrictions. Experimental values of λ_{111} measured at room temperature are given in table 5 for the binary compounds SmFe₂, TbFe₂, DyFe₂ (see section 6), HoFe₂, ErFe₂ and TmFe₂.

It is clear from the foregoing that since in many cases $\lambda_{111} \gg \lambda_{100}$, care must be taken in interpreting measurements on polycrystals. Typical preparation techniques yield samples which are far from isotropic. Crystallites grow anisotropically, most rapidly along a direction near [211] (McMasters unpublished).

4. Magnetization and sublattice magnetization of RFe₂ compounds

Magnetization measurements on a large number of RFe₂ binary and pseudo-binary polycrystals have been reported on the literature. Extensive measurements over a wide range of temperatures have been made by Buschow and Van Stapele (1970, 1971) and Burzo (1971). It is clear from this work and the earlier work of Wallace and Skrabek (1964) that the rare earth and iron moments couple antiferromagnetically. Within the last few years, magnetization measurements in high fields and on single crystals have become available (Clark et al. 1974, 1977, 1978, Abbundi et al. 1979). In this section, comparison will be made between single crystal and polycrystal data. Single crystal magnetizations will be used to calculate theoretical temperature dependences of the magnetostriction utilizing a theory formulated by Callen and Callen (1963).

In figs. 14 through 18, the magnetic moment along the easy magnetization direction is compared to data taken on polycrystalline samples for TbFe₂, DyFe₂, HoFe₂, ErFe₂ and TmFe₂. Although the compounds are cubic and only moderate anisotropies were initially expected, it is clear that the full saturation magnetization is not achieved in any of the polycrystal specimens at low temperatures. Instead, large cubic anisotropies were measured in all compounds (see section 5). The easy directions of magnetization are consistent with those predicted by the earlier Mössbauer measurements (Wertheim et al. 1964, Bowden et al. 1968, Guimaraes 1971, Atzmony et al. 1973). In a polycrystal in which crystallites are distributed uniformly over all directions, if the [111] axis is easy, and if the magnetization lies along the [111] axis in each crystallite closest to the external field, the polycrystal remanent moment is 0.866 of the aligned saturation moment (Chikazumi and Charap 1964). This is close to the observed polycrystal/single crystal

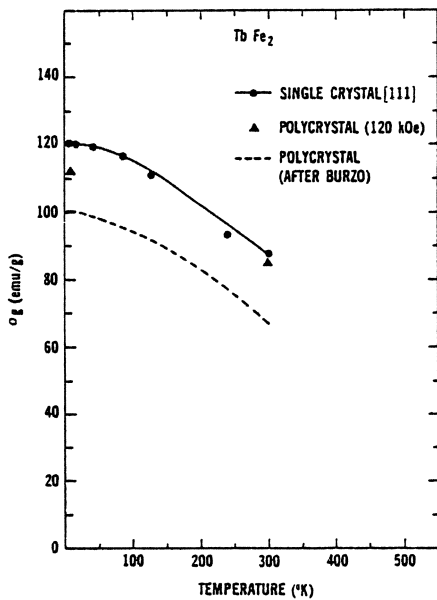


Fig. 14. Magnetic moment of TbFe₂ (taken from Clark et al. 1978, Burzo 1971).

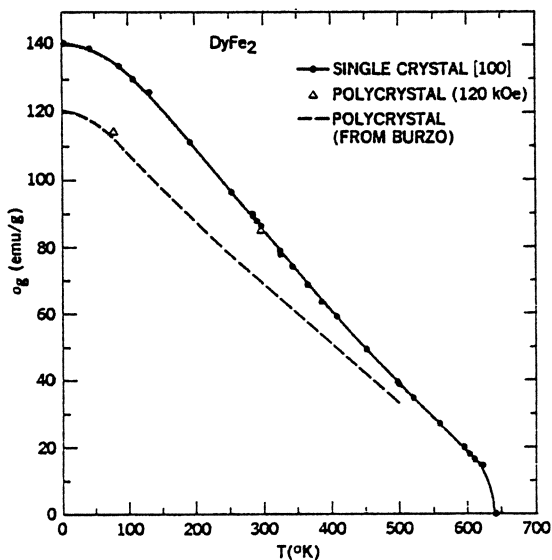


Fig. 15. Magnetic moment of DyFe₂ (taken from Clark et al. 1978, Burzo 1971).

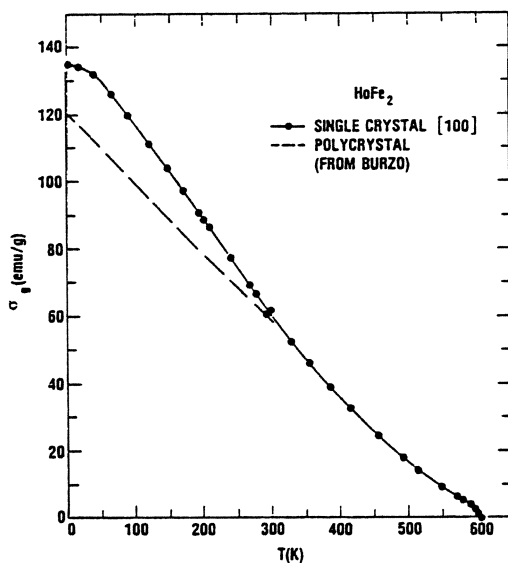


Fig. 16. Magnetic moment of HoFe_2 (taken from Abbundi et al. 1979, Burzo 1971).

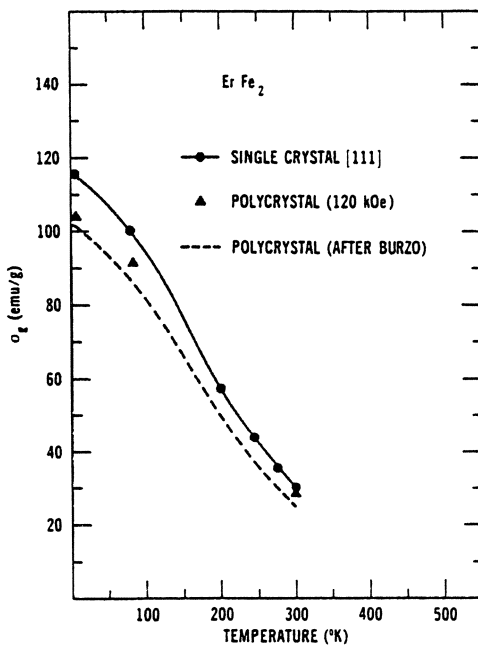


Fig. 17. Magnetic moment of ErFe_2 (taken from Clark 1974, Burzo 1971).

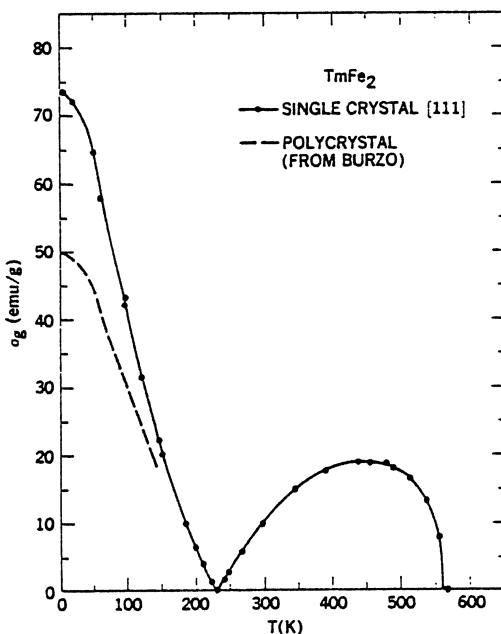


Fig. 18. Magnetic moment of TmFe₂ (taken from Clark et al. 1978, Burzo 1971).

moment ratio at 4 K for TbFe₂ and ErFe₂. When [100] is easy, the corresponding calculated ratio is 0.832. In DyFe₂ and HoFe₂, the ratios are ~ 0.87 , only slightly higher than the calculated value. No moments have been reported to date for single crystal SmFe₂. In table 6 are collected Curie temperatures, atomic magnetic moments, magnetizations and theoretical densities for these compounds. Similar values of iron sublattice moments ($1.61 \pm 0.04\mu_B$) at 0 K are calculated from the single crystal magnetization measurements assuming that the rare earth moments equal gJ . They are remarkably close to those adduced from nuclear hyperfine fields by Wallace (1968).

Unlike the magnetostrictions of the transition metals Ni, Co and Fe, the magnetostrictions of the rare earth elements follow a rather simple single-ion temperature dependence. Callen and Callen (1963, 1965) developed a formulation which directly relates the temperature dependence of the magnetostriction to the temperature dependence of the rare earth magnetization. This formulation is valid in the molecular field approximation, spin wave approximation and various Green's function theories (Callen and Shtrickman 1965). They find

$$\lambda^{\mu,l}(T) = \lambda^{\mu,l}(0) \hat{I}_{l+1/2}(x) \quad (4.1)$$

where $\hat{I}_{l+1/2}$ is the ratio of the hyperbolic Bessel function of order $l + \frac{1}{2}$ to the hyperbolic Bessel function of order $\frac{1}{2}$. The argument x is related to the normalized magnetization $m = M/M_s$ through the relationship

TABLE 6
Magnetic moments and Curie temperatures of $R\text{Fe}_2$

$R\text{Fe}_2$	$\sigma(\text{emu/g})$		ρ g/cm^3	$M(\text{emu/cm}^3)$		n_b 0 K	$n_{b\text{Fe}}$ 300 K	$n_{b\text{Fe}}$ η	T_c K
	0 K	300 K		0 K	300 K				
$\text{TbFe}_2^{\text{a)}}$	120	88	9.06	1090	800	5.81	4.26	1.60	1.75
$\text{DyFe}_2^{\text{b)}}$	140	87	9.28	1300	810	6.87	4.27	1.57	1.60
$\text{HoFe}_2^{\text{c)}}$	135	62	9.44	1274	590	6.70	3.06	1.65	1.55
$\text{ErFe}_2^{\text{b)}}$	116	29	9.62	1120	280	5.79	1.45	1.61	1.60
$\text{TmFe}_2^{\text{a)}}$	74	10	9.79	725	98	3.72	0.49	1.64	1.55
$\text{SmFe}_2^{\text{d)}}$	48	47	8.53	410	400	2.25	2.20	—	560
									676

^{a)} Taken from single crystal data (Clark et al. 1978).

^{b)} Taken from single crystal data (Clark 1974 Clark et al. 1978).

^{c)} Taken from single crystal data (Abbundi et al. 1979).

^{d)} Taken from polycrystal data (Buschow, unpublished).

^{e)} Calculated from single crystal data assuming $n_{b\text{Fe}} = gJ$.

^{f)} Calculated from Mössbauer spectra (see Wallace 1968).

^{g)} Taken from polycrystal data (Buschow and Van Stapele 1971, Burzo 1971).

$$m = \hat{I}_{3/2}(x). \quad (4.2)$$

Since $\hat{I}_{3/2}$ is the familiar Langevin function, $\mathcal{L}(x) = \coth x - 1/x$, $\hat{I}_{l+1/2}$ ($l > 1$) can be considered to be "higher order" Langevin functions (Callen and Callen 1965, Keffer 1955). In molecular field theory, $x = \mu H/kT$, where μ is the magnetic moment/ion and H is the total (effective + external) magnetic field. In a more general sense, however, x can be defined through eq. (4.2). Thus, expressing the magnetostriction in terms of the normalized magnetization $m(T, H)$

$$\lambda^{\mu,l}(T) = \lambda^{\mu,l}(0)\hat{I}_{l+1/2}[\mathcal{L}^{-1}(m(T, H))]. \quad (4.3)$$

For the lowest order ($l = 2$) magnetostriction, e.g. λ_{100} and λ_{111} , we find $\lambda^{\mu,2}(T) = \lambda^{\mu,0}(0)m^3(T)$ at low temperatures and $\lambda^{\mu,2}(T) \approx 0.6\lambda^{\mu,2}(0)m^2(T)$ at high temperatures. The functional dependence of $\hat{I}_{l+1/2}$ on m is given for $l = 2, 4$ and 6 in Appendix B. To test the applicability of eq. (4.3) to the $R\text{Fe}_2$ compounds, the rare earth sublattice magnetizations, m_R 's, must be known.

These sublattice magnetizations, m_R 's, can be obtained directly by Mössbauer and by neutron diffraction methods, and indirectly by subtracting the Fe magnetization from the total magnetization. The results are shown in fig. 19. For DyFe_2 good agreement is found between the values of m_{Dy} calculated from Mössbauer measurements (Bowden et al. 1968) and those obtained from the total magnetization measurements (Clark 1974). Similarly, good agreement is found between the neutron diffraction results (Rhyne, unpublished) and total magnetization results for HoFe_2 (Abbundi et al. 1979) and ErFe_2 (Clark 1974). For TbFe_2 the neutron diffraction data (Rhyne, unpublished) is higher than that calculated from the magnetization over the entire temperature range. Both these measurements, however, fall within the uncertainty cited by Barbara et al. (1977) in their neutron diffraction data on TbFe_2 . For TmFe_2 the neutron diffraction

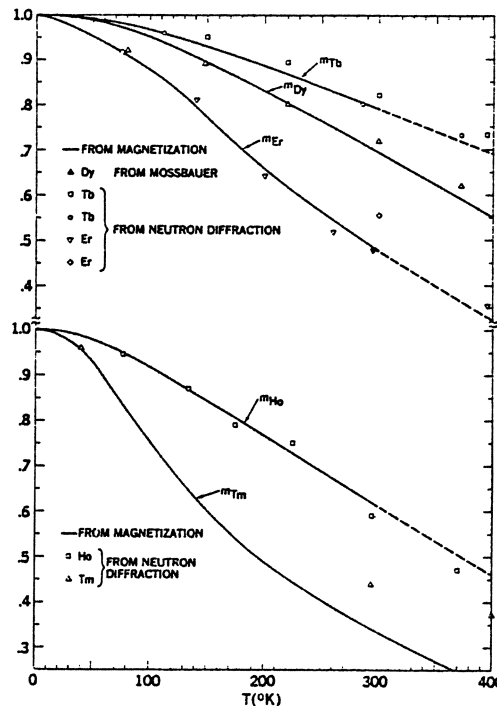


Fig. 19. Normalized rare earth sublattice magnetizations in $R\text{Fe}_2$. (Δ (Mössbauer) Bowden et al. 1968; $\square \nabla \Delta$ Rhyne, unpublished, \circ Barbara et al. 1977, \diamond Bargouth and Will 1971). The solid lines were calculated from single crystal magnetizations minus the iron sublattice magnetizations (Bowden et al. 1968) normalized to the respective Curie temperatures of the compounds.

data (Rhyne, unpublished, Barbara et al. 1977) are not in agreement with the total magnetization results, leading to incorrect magnetizations and compensation temperatures. Thus the currently available neutron diffraction data for TmFe_2 are considered unsatisfactory.

The temperature dependence of the magnetostrictions were calculated from eq. (4.3) using the rare earth sublattice magnetizations of fig. 19. Excellent agreement between the measured temperature dependences and those calculated from the lowest order ($l = 2$) single-ion theory were found for TbFe_2 (fig. 10) and TmFe_2 (fig. 11). The Callen-Callen single-ion theory was found insufficient to account for the (small) λ_{100} of DyFe_2 and HoFe_2 (fig. 9 and 10).

5. Magnetic anisotropy of binary $R\text{Fe}_2$ compounds

The largest magnetic anisotropies occur in uniaxial crystals. The hexagonal rare earth elements possess the largest known magnetic anisotropies at low temperatures. The high Curie temperature compounds $R\text{Co}_5$ and $R_2\text{Co}_{17}$ possess the

largest known magnetic anisotropy energies at room temperature. Smaller anisotropies are found in the cubic RFe_2 compounds. However, recent measurements have shown that they possess by far the largest known anisotropies of cubic crystals. Depending upon the strength of the rare earth-iron exchange, this large anisotropy sometimes persists to room temperature.

Anisotropy constants were experimentally determined by both magnetization and magnetic torque measurements on single crystals of the binary RFe_2 compounds (Clark et al. 1973, 1978, Williams and Koon 1975). The room temperature anisotropy constants K_1 of $TbFe_2$, $DyFe_2$, $HoFe_2$, $ErFe_2$ and $TmFe_2$ are compared to some typical cubic ferro- and ferrimagnets in table 7. The decrease in Curie temperature with increasing atomic number is directly reflected in the room temperature value of the rare earth sublattice magnetization m_R (fig. 19) and thus in the magnitude of the room temperature magnetic anisotropy. In $TbFe_2$, anisotropy fields are in excess of 100 kOe at room temperature, while in $TmFe_2$, saturation is achieved below 12 kOe (see fig. 20). The easy axes are consistent with the earlier Mössbauer spectra measurements (see compilation by Taylor 1971).

The total anisotropy is a sum of both intrinsic and magnetoelastic contributions (see section 2). In table 8 are shown the calculated contributions to the anisotropy from the magnetoelastic coupling, as obtained from $\Delta K_1 = -\frac{9}{2}c_{44}\lambda_{111}^2$. Subtracting these values from the total anisotropies of table 7, the intrinsic anisotropies $K_1^{int}(300)$ and $K_1^{int}(0)$ were inferred. For $TbFe_2$, $DyFe_2$ and $TmFe_2$, where the intrinsic magnetostriction, $\alpha J(J-\frac{1}{2})$ is large, $\Delta K_1(300)/K_1(300) \approx 20\%$; for $HoFe_2$ and $ErFe_2$, where the magnetostriction is smaller, $\Delta K_1(300)/K_1(300) \leq 6\%$.

According to single-ion theory (see Appendix B), the temperature dependence

TABLE 7
Anisotropy constants of some cubic metals and ferrites at room temperature

Metal	$10^{-4}K_1(\text{ergs/cm}^3)$	Ferrite	$10^{-4}K_1(\text{ergs/cm}^3)$
Fe	45 ^{a)}		
Ni	-5 ^{a)}		
70% Fe-Co	-43 ^{b)}	$Ga_{0.44}Fe_{2.54}O_4$	-81 ^{c)}
65% Co-Ni	-26 ^{c)}	$CoFe_2O_4$	260 ^{b)}
$TbFe_2$	-7600 ^{d)}	$Co_{0.8}Fe_{2.2}O_4$	290 ^{b)}
$DyFe_2$	2100 ^{d)}	$Co_{0.5}Zn_{0.2}Fe_{2.3}O_4$	150 ^{b)}
$HoFe_2$	580 ^{e)} , 550 ^{f)}		
$ErFe_2$	-330 ^{d)}		
$TmFe_2$	-53 ^{f)}		

^{a)} Hoffman (1967).

^{b)} Abbundi and Clark (1978).

^{b)} McKeehan (1937).

^{b)} Pearson (1960).

^{c)} Shih (1936).

^{b)} Perthel et al. (1966).

^{d)} Clark et al. (1972, 1975).

^{b)} Bozorth et al. (1955).

^{e)} Williams et al. (1978).

^{b)} Abbundi et al. (1979).

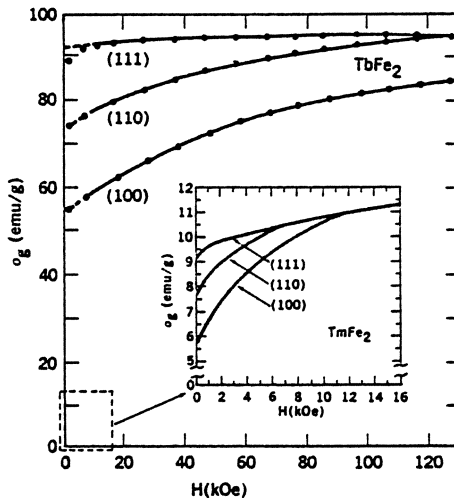


Fig. 20. Magnetic moment of TbFe₂ and TmFe₂ at room temperature (taken from Clark et al. 1975, Abbundi and Clark 1978).

TABLE 8
Intrinsic, K_1^{in} , and magnetoelastic, ΔK_1 , contributions to the magnetic anisotropy (ergs/cm³)

RFe ₂	$\Delta K_1(300)^*$ $\times 10^{-4}$	$K_1^{\text{in}}(300)$ $\times 10^{-4}$	$\frac{\Delta K_1(300)}{K_1^{\text{in}}(300)}$	$K_1^{\text{in}}(0)^{**}$ $\times 10^{-8}$
SmFe ₂	-970	-	-	-
TbFe ₂	-1330	-6300	0.21	-5.2
DyFe ₂	-350	2450	-0.14	4.7
HoFe ₂	-7.5	590	-0.01	2.7
ErFe ₂	-20	-310	0.06	-5.4
TmFe ₂	-9.7	-43	0.22	-3.8

* Calculated from $\frac{9}{2}c_{44}\lambda_{111}^2$ taking $c_{44} = 4.87 \times 10^{11}$ dynes/cm² from Rinaldi et al. (1977).

** Extrapolated to $T = 0$ using single-ion theory.

of the lowest order (intrinsic) anisotropy constant in cubic crystals is given by

$$K^{\alpha,4}(T)/K^{\alpha,4}(0) = \hat{I}_{9/2}[\mathcal{L}^{-1}(m_R)] \quad (5.1)$$

or

$$K_1(T)/K_1(0) = \hat{I}_{9/2}[\mathcal{L}^{-1}(m_R)] \quad (5.2)$$

whenever $|K_2| \ll |11 K_1|$.

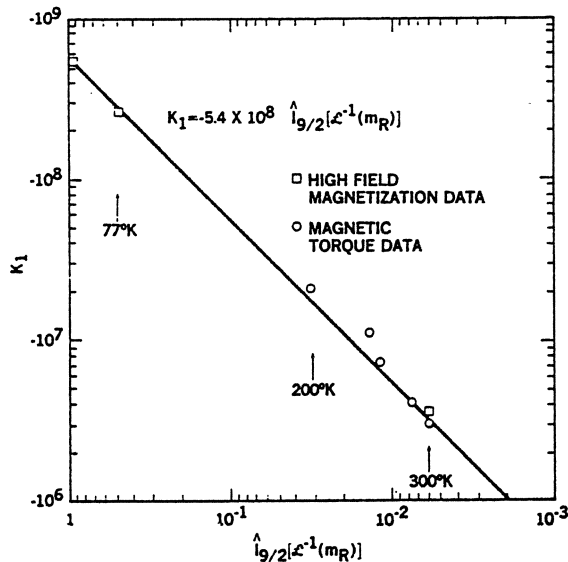


Fig. 21. Magnetic anisotropy K_1 of ErFe_2 vs. single-ion theory (taken from Clark et al. 1974).

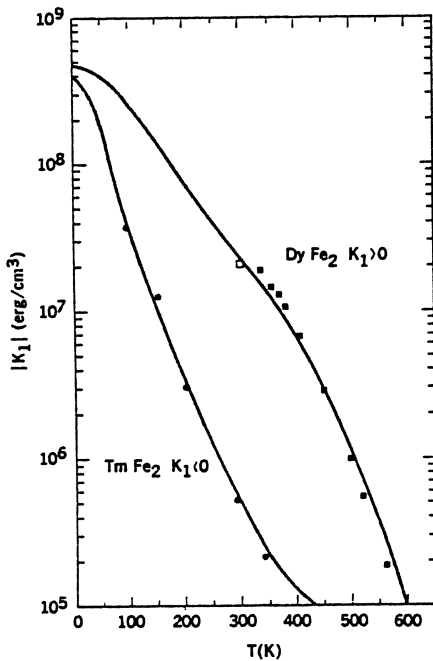


Fig. 22. Anisotropy constant K_1 for DyFe_2 and TmFe_2 as a function of temperature (taken from Clark et al. 1978). The solid curves are calculated from single-ion theory.

Figure 21 shows that the experimentally observed anisotropy of ErFe₂, in which $\Delta K/K$ is negligible, conforms rather well to the simple theory, as given by eq. (5.2). The temperature dependence of the anisotropy constants (K_{\dagger}) for DyFe₂ and TmFe₂ are plotted in fig. 22. The anisotropy spans three decades. Again satisfactory agreement between experiment and theory is found. With one adjustable constant, $K_{\dagger}^{\text{int}}(0)$, the fit to the data is within 20% over the entire temperature range. The values of $K_{\dagger}^{\text{int}}(0)$ calculated from eq. (5.2), utilizing higher temperature measured values and the sublattice magnetizations m_R from section 4, are given in table 8. All anisotropy magnitudes exceed 2×10^8 erg/cm³ at $T = 0$ K and agree with each other within a factor of two.

Higher order anisotropy terms also contribute to the total anisotropy energy, particularly at low temperatures. Evidence for their existence can be found from spin reorientation diagrams of pseudobinary RFe₂ compounds (Atzmony et al. 1973, 1977; Atzmony and Dariel 1976) and from torque magnetometry measurements in the Tb_xHo_{1-x}Fe₂ system (Williams and Koon 1975, 1978). Temperature dependences of the anisotropy constants are in general complex and require the inclusion of the large magnetoelastic contribution (Koon and Williams 1978).

The binary RFe₂ compounds TbFe₂, DyFe₂, HoFe₂, ErFe₂ and TmFe₂ have only one easy direction at all temperatures. However anisotropy compensation and spin reorientation can be achieved with suitable rare earth alloying into compounds of the form $R_x^{(1)}R_y^{(2)}\dots Fe_2$ ($x + y \dots = 1$). Spin reorientation diagrams and anisotropy measurements for some pseudobinary RFe₂ compounds are discussed in section 6.

6. Magnetostriiction of pseudobinary RFe₂ compounds

In the hexagonal rare earths, the lowest order anisotropy and magnetostriiction arises from the same degree of spin operator ($l = 2$). In contrast, in the RFe₂ compounds, because they are cubic, the anisotropy arises from $l = 4$ terms and the magnetostriiction from $l = 2$ terms. This makes it possible to tailor compounds with optimum magnetostriiction and anisotropy properties simultaneously. For certain magnetostriuctive materials applications, high strains at low fields are necessary. In these cases a low anisotropy is important in order to maximize domain wall mobility and easy domain rotation at low fields.

Table 9 shows the signs of λ , $K^{\alpha,4}$ and $K^{\alpha,6}$ for the binary RFe₂ compounds taken from the signs of the Stevens' equivalent operator coefficients. Using this table, pseudobinary compounds can be constructed in such a way as to minimize the magnetic anisotropy while still maintaining a large positive (or negative) magnetostriiction. It is preferable to alloy binary compounds with the same magnetostriiction sign but with opposite signs of anisotropy. Ternary compounds yielding large positive magnetostrictions at room temperature must contain Tb. Hence acceptable anisotropy compensating systems are Tb_{1-x}Dy_xFe₂, Tb_{1-x}Ho_xFe₂ and Tb_{1-x}Pr_xFe₂. Experimental spin reorientation diagrams for Tb_{1-x}Dy_xFe₂ and Tb_{1-x}Ho_xFe₂ are shown in fig. 23. The region of

TABLE 9
Polarity of λ , $K^{a,4}$ and $K^{a,6}$

	$\text{PrFe}_2^{\text{a)}}$	SmFe_2	TbFe_2	DyFe_2	HoFe_2	ErFe_2	TmFe_2	$\text{YbFe}_2^{\text{a)}}$
λ	+	-	+	+	+	-	-	-
$-K^{a,4}, K_1 + K_2/11$	+	-	-	+	+	-	-	+
$K^{a,6}, K_2$	-	0	+	-	+	-	+	-

^{a)}The binary PrFe_2 and YbFe_2 compounds are not readily synthesized.

spin reorientation and anisotropy compensation are clearly identified from 0 K to 300 K. Ternary compounds possessing a large negative magnetostriction at room temperature must possess Sm. However Yb, the only suitable element with the correct sign distribution, is not available in a trivalent state. Fortunately, the ratio of λ/K is much larger for Sm than for the heavy rare earth compounds.

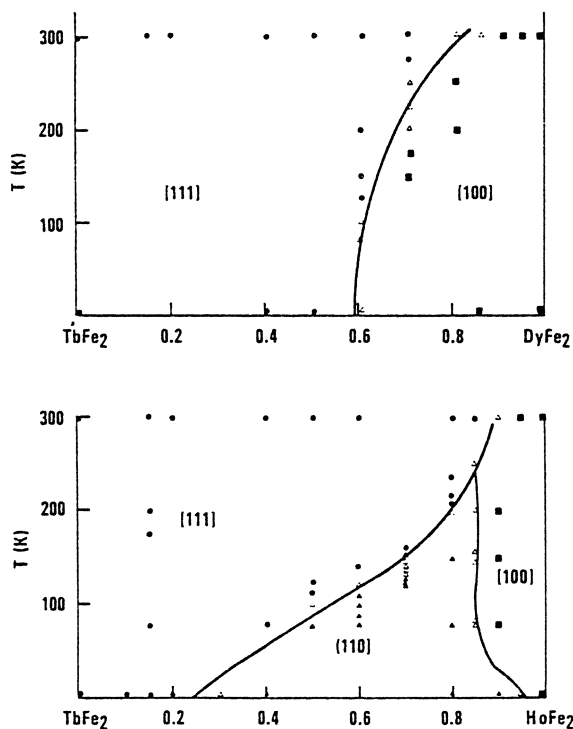


Fig. 23. Spin orientation of $\text{Tb}_{1-x}\text{Dy}_x\text{Fe}_2$ and $\text{Tb}_{1-x}\text{Ho}_x\text{Fe}_2$ systems (taken from Atzmony et al. 1973). Filled circles, triangles and squares correspond to [111], [110] and [100] axes of magnetization respectively. Open triangles correspond to intermediate directions.

Hence certain ternary alloys, such as Sm_{1-x}Dy_xFe₂ and Sm_{1-x}Ho_xFe₂, are attractive candidates for anisotropy minimization.

The Tb_{1-x}Dy_xFe₂ system has been investigated in detail. In fig. 24, are shown the magnetostrictions at room temperature of polycrystalline samples of Tb_{1-x}Dy_xFe₂ for $H = 10$ kOe and $H = 25$ kOe. Near $x = 0.7$, the magnetostrictions at these fields exhibit a peak, reflecting the near zero magnetic anisotropy at this concentration. Figure 25 illustrates how the single crystal magnetostriction constant λ_{111} varies with Dy concentration. λ_{111} was determined by X-ray techniques, utilizing a method developed (Dwight and Kimball 1974, Clark et al. 1975) to accurately determine the magnetostriction at the point of spin reorientation. When [111] is easy, a large rhombohedral distortion (λ_{111}) occurs contributing to a large X-ray splitting of the (440) and (620) lines. When [100] is easy, only a tiny distortion is realized ($\lambda_{100} \approx 0$) and X-ray splittings are not observed. The concentration at which the magnetostriction disappears clearly identifies the point of anisotropy minimization. At the spin reorientation $\lambda_{111} = 1600 \times 10^{-6}$. The extrapolated value of λ_{111} for DyFe₂ is 1260×10^{-6} .

The magnetostriction of single crystal Tb_{0.27}Dy_{0.73}Fe₂ has been measured through the anisotropy compensation region (Abbundi and Clark 1977). A spectacular "turning on" of a huge rhombohedral (magnetostrictive) strain by a rise in temperature occurs. At low temperatures, $M \parallel [100]$, and no significant

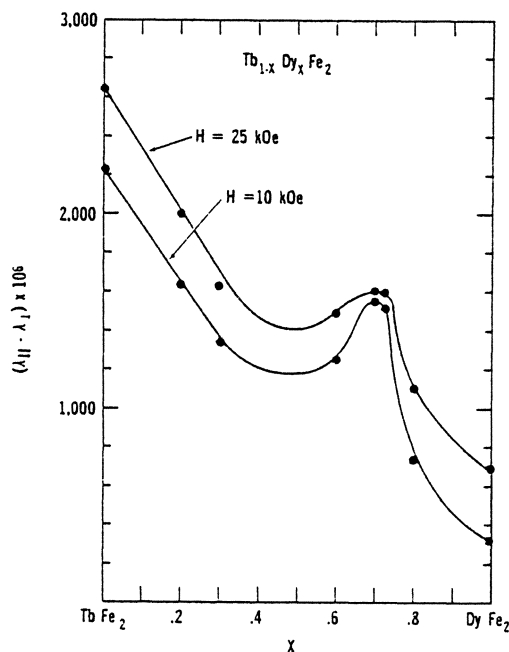


Fig. 24. Magnetostriction of Tb_{1-x}Dy_xFe₂ at room temperature (taken from Clark 1974).

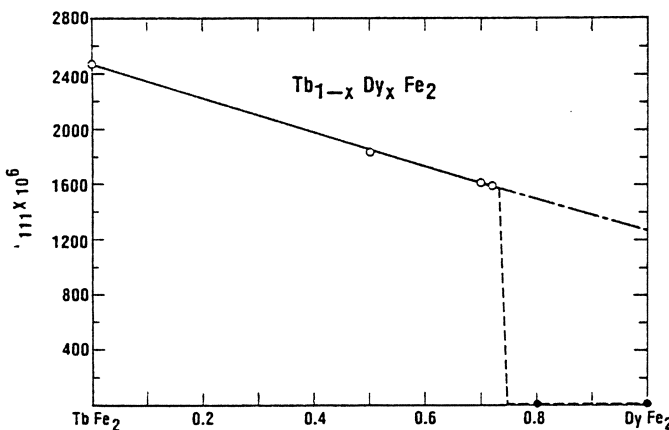


Fig. 25. λ_{111} of $Tb_{1-x}Dy_xFe_2$ at room temperature. Open circles are λ_{111} ; solid circles denote region where no spontaneous λ_{111} exists (taken from Clark et al. 1976).

magnetostrain exists. Rather abruptly, at the anisotropy compensation temperature, magnetization rotation takes place and a large rhombohedral distortion (λ_{111}) develops. The effective linear thermal expansion coefficient $\alpha_e = d\lambda_{111}/dT$ reaches 110 ppm in this region (see fig. 26). The region of the anomalous thermal expansion can be shifted in temperature by application of an external magnetic field. The fields required for magnetization saturation through the compensation region are shown in fig. 27.

In fig. 28, the room temperature saturation magnetostriction measurements of Koon et al. (1974) for $Tb_{1-x}Ho_xFe_2$ are shown as a function of composition x . Since the anisotropy of Ho is smaller than that of Dy at room temperature, compensation occurs at a larger value of x than in the $Tb_{1-x}Dy_xFe_2$ system. In $Tb_{1-x}Ho_xFe_2$, compensation occurs near $x = 0.85$ as indicated by the anisotropy measurements of Williams and Koon (1975). At this concentration, $\lambda_{111} = 500 \times 10^{-6}$ (Koon and Williams 1977).

Figure 29 shows the effect of the addition of $PrFe_2$ to $TbFe_2$. Here the magnetostriction remains very high, but complete anisotropy compensation cannot be reached. Beyond 20% substitution, non-cubic phases appear.

In multicomponent pseudobinary systems, such as $Tb_xDy_yHo_zFe_2$, $Tb_xDy_yPr_zFe_2$ and $Tb_xDy_yHo_zPr_wFe_2$, values of x , y , z and w can be selected to achieve maximum magnetostriction with the simultaneous minimization of two or more anisotropy constants. Williams and Koon (1977) have successfully determined the alloy composition of the $(Tb_{0.3}Dy_{0.7}Fe_2)_x(Tb_{0.14}Ho_{0.86}Fe_2)_{1-x}$ pseudobinary for simultaneously minimization of the two lowest order anisotropy constants. They found low anisotropy for $x = 0.32$ and calculated a still lower anisotropy for $Tb_{0.20}Dy_{0.22}Ho_{0.58}Fe_2$. For this compound, $\lambda_s = 530 \times 10^{-6}$. The three lowest symmetry anisotropy constants κ_4 , κ_6 and κ_8 , calculated from a least square fit to torque data, are illustrated in fig. 30.

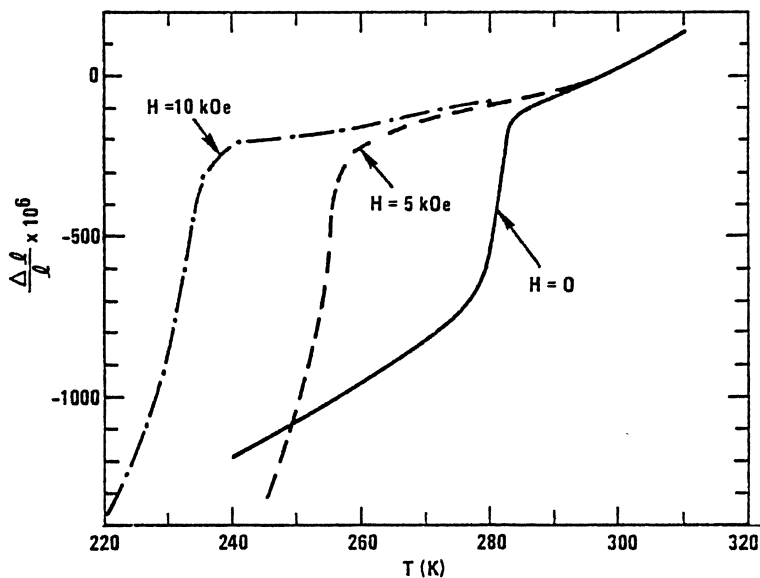


Fig. 26. Thermal expansion along [111] in single crystal $Tb_{0.27}Dy_{0.73}Fe_2$ (taken from Abbundi and Clark 1977).

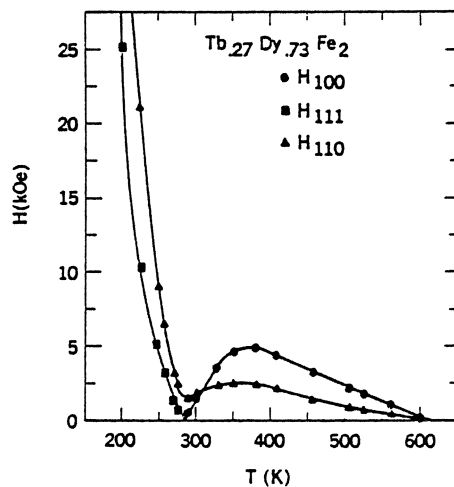


Fig. 27. Fields required for magnetic saturation along the principal directions in single crystal $Tb_{0.27}Dy_{0.73}Fe_2$ (taken from Clark et al. 1978).

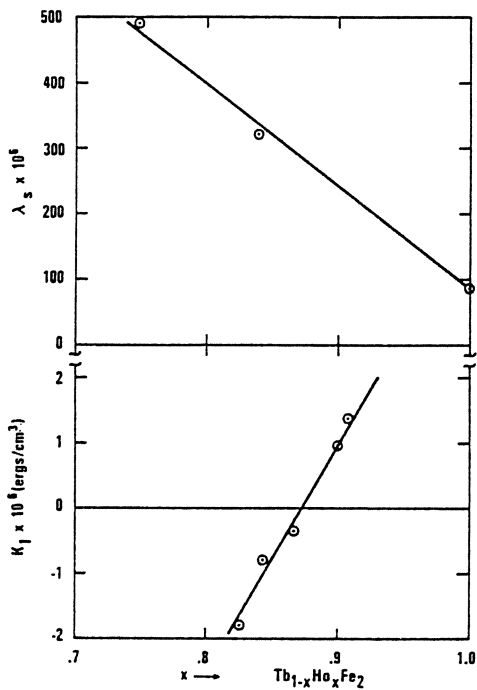


Fig. 28. Magnetostriction, λ_s , and magnetic anisotropy of $Tb_{1-x}Ho_xFe_2$ (taken from Koon et al. 1974, Williams, private communication).

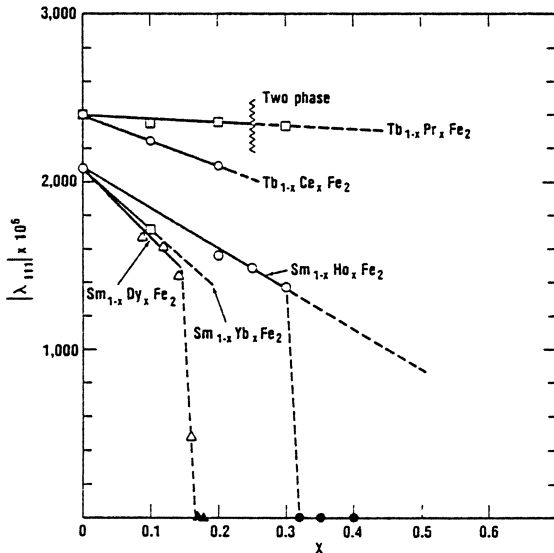


Fig. 29. λ_{III} of some $Tb_{1-x}R_xFe_2$ and $Sm_{1-x}R_xFe_2$ alloys. Open symbols are $|\lambda_{III}|$; solid symbols denote region where no spontaneous λ_{III} exists (taken from Clark et al. 1977).

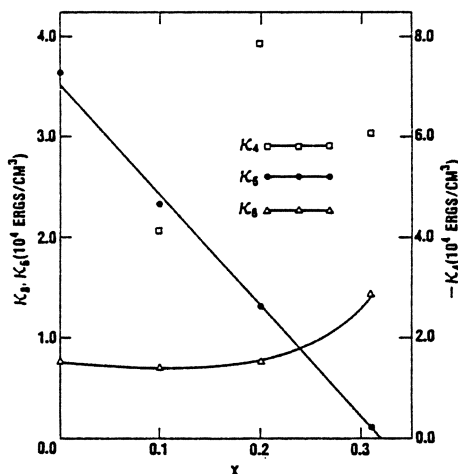


Fig. 30. Anisotropy constants κ_4 , κ_6 and κ_8 for the compound $(\text{Ho}_{0.86}\text{Tb}_{0.14}\text{Fe}_2)_{1-x}(\text{Dy}_{0.7}\text{Tb}_{0.3}\text{Fe}_2)_x$ (taken from Williams and Koon 1977).

Values of the magnetostriction for some quaternary compounds are listed in table 13 of section 8.

In fig. 29, the absolute value of λ_{111} is plotted vs. x ($0 < x < 0.4$) for the two Sm alloys $\text{Sm}_{1-x}\text{Dy}_x\text{Fe}_2$ and $\text{Sm}_{1-x}\text{Ho}_x\text{Fe}_2$. In these systems, both λ_{111} and K_1 compensate, as can be seen from the sign distribution in table 9. However, because of the relatively small anisotropy of SmFe_2 , only small additions of Dy and Ho are needed for spin reorientation and anisotropy minimization. X-ray measurements show that reorientation occurs near $x = 0.12$ for $\text{Sm}_{1-x}\text{Dy}_x\text{Fe}_2$ and near $x = 0.3$ for $\text{Sm}_{1-x}\text{Ho}_x\text{Fe}_2$. The values of magnetostriction at these concentrations are large and negative. In both alloys, $|\lambda_{111}| > 1200 \times 10^{-6}$.

RFe₂ bimetallic strips composed of highly magnetostrictive alloys of both positive and negative polarity can exhibit huge flexural strains. The extent of the motion depends upon the magnetostrictions, strip length and strip thickness.

7. Elastic properties of RFe₂ compounds

Room temperature sound velocities, densities and moduli are listed in table 10 for polycrystalline TbFe₂, ErFe₂, YFe₂ and TbFe₃. The moduli are midway between those of the soft rare earth elements and the stiffer magnetic transition metals, such as Fe and Ni. The moderate magnitudes of the moduli and the huge magnitudes of the magnetostrictions combine to yield huge magnetoelastic forces and energies for these compounds. Values of λ_s , $E\lambda_s$ and the energy density, $\frac{1}{2}E\lambda_s^2$, are shown in table 10. They are compared to those of elemental Ni, a typical magnetostrictive material. The quantity $E\lambda_s$ is a measure of the pressure exerted by a constrained bar of the material which is magnetized to

TABLE 10
Elastic and magnetoelastic properties^{a)}

	TbFe ₂	ErFe ₂	YFe ₂	TbFe ₃	Ni
v_t (m/sec)	3940	4120	4340	4230	-
v_s (m/sec)	1980	2180	2720	2320	-
ρ (g/cm ³)	9.1	9.7	6.7	9.4	-
$E \times 10^{-10}$ (newton/m ²)	9.4	12.1	12.7	13.1	21 ^{b)}
$\lambda_s \times 10^6$	1750	-229	-	693	-31 ^{c)}
$E\lambda_s \times 10^{-7}$ (newton/m ²)	17	2.8	-	9	0.7
$E\lambda_s^2/2 \times 10^{-3}$ (joule/m ³)	145	3.2	-	32	0.1

^{a)} Clark et al. (1973b).

^{b)} "Nickel". The International Nickel Co., Inc. (1951).

^{c)} Went (1951).

saturation. The energy density, $\frac{1}{2}E\lambda_s^2$, represents the amount of magnetic energy which can be transformed to elastic energy per unit volume of the material. For TbFe₂ this energy is about 1000 times that of earlier magnetostrictive materials, such as Ni.

Rosen et al. (1973, 1974) have determined the Young's modulus and the shear modulus ultrasonically for the ternary Tb_{1-x}Ho_xFe₂ system and for SmFe₂ as a function of temperature. Their values are illustrated in fig. 31. Clearly defined depressions in the moduli occur where easy axis rotation takes place. (Refer to the spin reorientation diagram of fig. 23 and the magnetostriction data of fig. 12.) Young's moduli for a large number of binary RFe₂ compounds as a function of temperature are given in fig. 32 (Klimker et al. 1974).

Unprecedented changes in elastic moduli with magnetic field (ΔE effect) have been observed in the highly magnetostrictive RFe₂ compounds. In figs. 33 and 34 are plotted the relative changes in Young's modulus with field, $E_H - E_0$, normalized to the modulus at zero field E_0 . ΔE effects are huge for the highly magnetostrictive TbFe₂ and Tb_{0.3}Dy_{0.7}Fe₂ compounds. Conventional ΔE effects, i.e. reductions in the modulus from their intrinsic high field values, have been generally associated with domain wall motion (see Bozorth 1951). However, in the RFe₂ compounds, the moduli continue to change far above technical saturation. Thus the major source of the field dependences cannot be attributed to the motion of domains, but to an intrinsic softening of the lattice due to local atomic magnetoelastic interactions. In this section we shall derive an expression for the softening in the shear modulus, c_{44} , by the second order contribution of the large magnetoelastic coupling, b_2 .

It was shown in section 2 that a magnetostrictive system, composed of magnetic anisotropy, magnetoelastic energy and elastic energy components leads to the equilibrium strains

$$\epsilon_{ij}^{eq} = -(b_2/c_{44}^0)\alpha_i\alpha_j \quad (7.1)$$

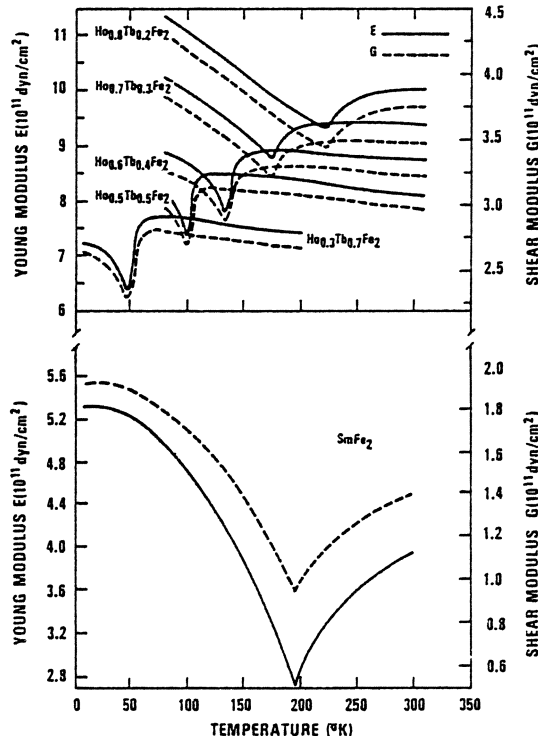


Fig. 31. Temperature dependence of Young's modulus, E , and shear modulus, G , for $\text{Tb}_{1-x}\text{Ho}_x\text{Fe}_2$ and SmFe_2 (taken from Rosen et al. 1973, 1974).

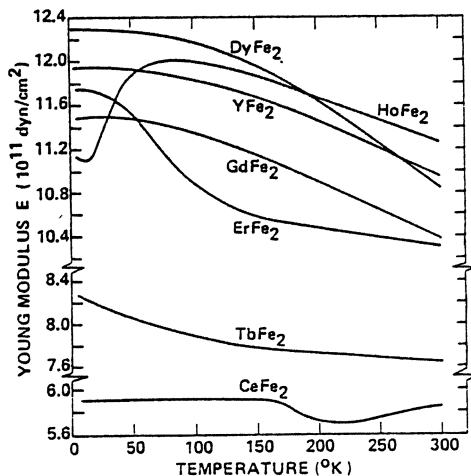


Fig. 32. Temperature dependence of the Young's moduli for the RFe_2 compounds (taken from Klimker et al. 1974).

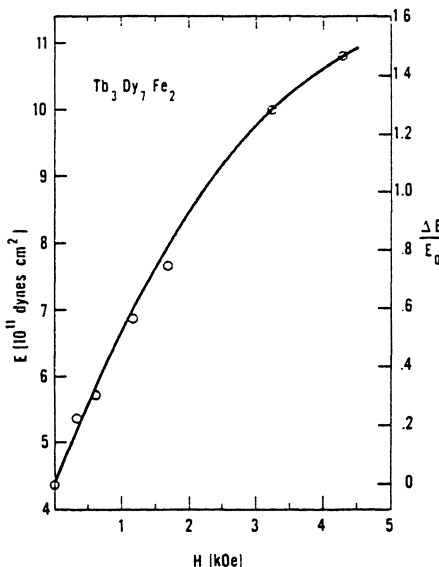


Fig. 33. Young's modulus and ΔE effect at room temperature for $Tb_{0.3}Dy_{0.7}Fe_1$, $\Delta E = E_H - E_0$ (taken from Clark and Savage 1975).

and to an effective anisotropy constant K'_1

$$K'_1 = K_1 - (b_2^2/2c_{44}^0) \quad (7.2)$$

whenever $b_2 \gg b_1$. (The superscript “ 0 ” is added to c_{44} to label the “intrinsic” stiffness.) Thus as a function of the magnetization cosines, α_i , the total energy at constant stress (including magnetoelastic and elastic terms) becomes simply

$$E^\sigma = K'_1(\alpha_x^2\alpha_y^2 + \alpha_y^2\alpha_z^2 + \alpha_x^2\alpha_z^2) + \text{constant} \quad (7.3)$$

The dependent variables, the strains, have been eliminated. Only an effective anisotropy constant remains.

In like manner the effect of the magnetoelastic interaction on the elastic moduli and sound velocity can be readily calculated. Here, instead of the strains, ϵ_{ij} , being the dependent variables, the magnetization direction cosines, α_i , are the dependent variables and the elastic strains are the independent variables. To determine c_{44} we consider an arbitrary ϵ_{xy} strain, produced, for example, by an ultrasonic transducer, and calculate the equilibrium values of α_x , α_y and α_z . This ϵ_{xy} strain can be visualized as a shear wave polarized in the x [100] crystalline direction and propagating in the y [010] direction. In the following we: (1) assume $b_2 \gg b_1$, and (2) introduce the effect of an external field applied along x , such that the moment is nearly parallel to x ($\alpha_x \approx 1$). For this case, the total energy expression [eq. (2.4)] becomes

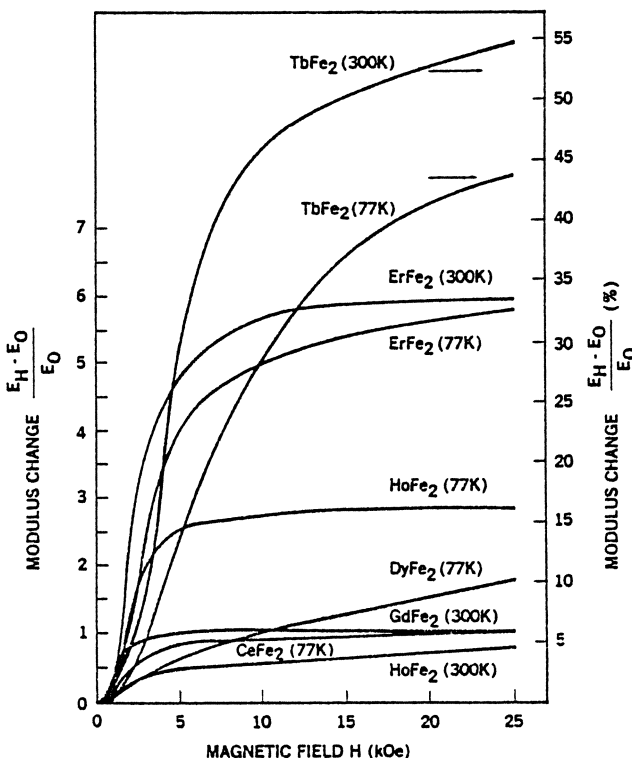


Fig. 34. Magnetic field dependence of the modulus change $(E_H - E_0)/E_0$ of the $R\text{Fe}_2$ compounds (taken from Klimker et al. 1974).

$$\begin{aligned} E = & K_1(\alpha_x^2 \alpha_y^2 + \alpha_y^2 \alpha_z^2 + \alpha_z^2 \alpha_x^2) - HM\alpha_x + b_2 \alpha_x \alpha_y \epsilon_{xy} + \frac{1}{2} C_{44}^0 \epsilon_{xy}^2 \\ & + b_2 (\alpha_y \alpha_z \epsilon_{yz}^{eq} + \alpha_z \alpha_x \epsilon_{zx}^{eq}) + \frac{1}{2} C_{44}^0 (\epsilon_{xz}^{eq 2} + \epsilon_{yz}^{eq 2}) \\ & + \text{elastic terms in } \epsilon_{xx}, \epsilon_{yy} \text{ and } \epsilon_{zz}. \end{aligned} \quad (7.4)$$

To determine the equilibrium values of α_i , the torque is set equal to zero. From the z component of the torque, it follows that

$$\alpha_x^{eq} \alpha_y^{eq} = - \frac{b_2}{2K_1 + MH} \epsilon_{xy}. \quad (7.5)$$

From the y component, it follows (to lowest order)

$$\alpha_z^{eq} = 0. \quad (7.6)$$

The equilibrium value α_x^{eq} can be approximated from eq. (7.5) using the relationship: $\alpha_x^2 = 1 - \alpha_y^2$. Thus

$$\alpha_x^{eq} \approx 1 - \frac{1}{2} \alpha_y^2 = 1 - \frac{1}{2} \frac{b_2^2}{(2K_1 + MH)^2} \epsilon_{xy}^2. \quad (7.7)$$

Substituting for $\alpha_x^{\text{eq}} \alpha_y^{\text{eq}}$ and for α_z^{eq} into eq. (7.4)

$$E = \frac{1}{2} \left(c_{44}^0 - \frac{b^2}{2K_1 + MH} \right) \epsilon_{xy}^2 - MH. \quad (7.8)$$

The coefficient of $\frac{1}{2}\epsilon_{xy}^2$, i.e. the effective elastic constant is

$$c_{44}^{\text{eff}} = c_{44}^0 - \frac{b^2}{2K_1 + MH}. \quad (7.9)$$

For large b^2/K_1 , the softening of the modulus can almost be complete. In terms of the measured anisotropy, K'_1 , eq. (7.9) becomes

$$\Delta c_{44} = c_{44}^0 - c_{44}^{\text{eff}} = c_{44}^0 \left(1 - \frac{K'_1}{K_1} \right) \left(\frac{1}{1 + MH/2K_1} \right). \quad (7.10)$$

The minimum c_{44} occurs when $K_1 = \frac{1}{2}b^2/c_{44}$, i.e. at the condition of magnetic isotropy ($K'_1 = 0$). Equation (7.10) is valid for $H \parallel$ shear polarization, p . For the case of $H \perp p$, there is no magnetoelastic effect to lowest order ($\alpha_z = 0$) and the elastic modulus c_{44} remains stiff. Note that in metals, where eddy currents play a significant role, H must be replaced by $H + 4\pi M$.

In fig. 35 is plotted $(c_{44}^0 - c_{44}^{\text{eff}})^{-1}$ vs. H as measured by Cullen et al. (1978) in $\text{Tb}_{0.3}\text{Dy}_{0.7}\text{Fe}_2$. Here H is applied parallel to the shear polarization, p . The large b_2 has a profound effect on c_{44} and the corresponding sound velocity. From eq. (7.9) it is possible to determine both b^2 and K_1 graphically. They find $|b_2| = 2.3 \times 10^9$ erg/cm³ and $K_1 = -3 \times 10^6$ erg/cm³, which are in excellent agreement with the static measurements reported in section 3. In fig. 36, the coupled ($H \parallel p$) and uncoupled ($H \perp p$) moduli are plotted vs. H . For the c_{44} mode, the reduction in the intrinsic modulus is $\sim 55\%$. The change in modulus is of the same order as

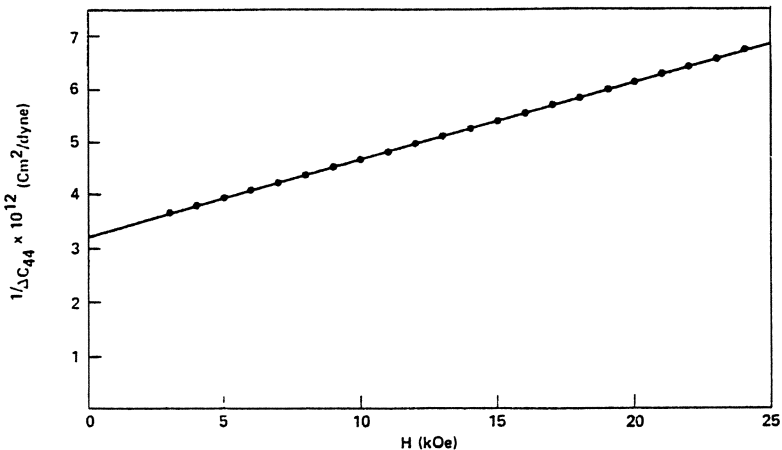


Fig. 35. The reciprocal of the difference in shear modulus, $1/(c_{44}^0 - c_{44})$ vs. magnetic field for $\text{Tb}_{0.3}\text{Dy}_{0.7}\text{Fe}_2$ (taken from Cullen et al. 1978).

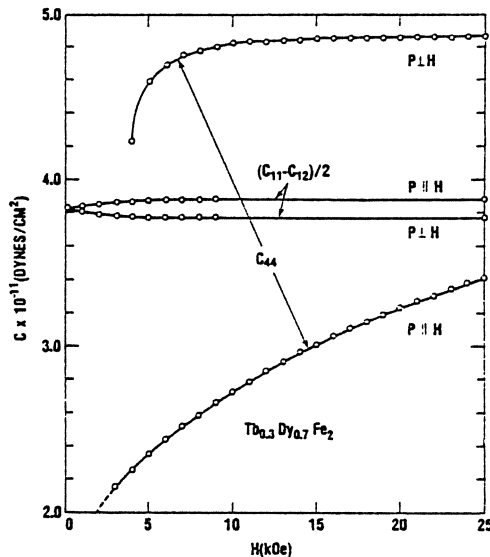


Fig. 36. Shear moduli c_{44} and $\frac{1}{2}(c_{11} - c_{12})$ for $\text{Tb}_{0.3}\text{Dy}_{0.7}\text{Fe}_2$ vs. magnetic field strength. The magnetic field was applied parallel and perpendicular to the shear polarization direction P (taken from Cullen et al. 1978).

the modulus itself. In contrast, the $\frac{1}{2}(c_{11} - c_{12})$ mode, for which the appropriate magnetoelastic coupling is b_1 , has a small magnetoelastic contribution. (In fact, for this case, the coupled modulus is higher than the uncoupled modulus. This cannot be attributed to the lowest order magnetoelastic effects considered above.) Note that $c_{44}^0 > \frac{1}{2}(c_{11} - c_{12}) > c_{44}^{\text{eff}}$ at low fields. Thus elastic isotropy can be achieved with $H \parallel p$ at a sufficiently large applied magnetic field. Elastic isotropy can also be achieved for lower fields applied along intermediate directions. Experiments on $\text{Tb}_{0.3}\text{Dy}_{0.7}\text{Fe}_2$ by Rinaldi et al. (1977) have shown that as a field H is rotated from $H \parallel p$ to $H \perp p$, the modulus rises smoothly from the lower strongly coupled value to the higher uncoupled value. Thus by rotation of the magnetic field, the elastic anisotropy can be nullified and even inverted, with the application of a very low applied magnetic field.

The uncoupled elastic constants as measured ultrasonically on $\text{Tb}_{0.3}\text{Dy}_{0.7}\text{Fe}_2$ by Rinaldi et al. (1977) are given in table 11.

In-depth studies of the magnetoelastic behavior of the shear moduli and the sound velocity have also been made in the polycrystalline $R\text{Fe}_2$ compounds at room temperature. Here, instead of a continuous change in shear modulus with field direction, the (degenerate) shear mode in the isotropic polycrystal breaks up into two modes, one polarized normal to the field and the other perpendicular (Cullen et al. 1978). Experimentally, two independent sound modes propagate whose intensities depend only upon field direction. Ultrasonic echo patterns taken for fields at various angles, θ , with respect to the direction of polarization of the

TABLE II
Elastic constants of $R\text{Fe}_2$ compounds* ($\times 10^{-11}$ dynes/cm 2)

	c_{11}	$\frac{1}{2}(c_{11} - c_{12})$	c_{44}^*
Dy Fe_2	14.58	3.89	4.70
Tb _{0.3} Dy _{0.7} Fe ₂	14.1	3.81	4.87

* Taken from Rinaldi et al. (1977, unpublished). c_{44} is a strong function of field. c_{44}^* denotes the pure (uncoupled) elastic modulus (see text).

impinging sound wave, are shown in fig. 37 for amorphous Tb Fe_2 . For $\theta = 0^\circ$ and 90° , a single train of echoes is observed with those for $\theta = 0^\circ$ reflecting the slower velocity. At intermediate angles, a superposition of the two patterns is observed, indicating the simultaneous propagation of two shear waves. The isotropy of the amorphous sample with respect to shear waves is broken by the magnetoelastic coupling.

The magnetic field dependences of both shear waves were measured in polycrystalline Tb_{0.27}Dy_{0.73}Fe₂, Sm_{0.88}Dy_{0.12}Fe₂, Sm_{0.7}Ho_{0.3}Fe₂ and amorphous Tb Fe_2 (a-Tb Fe_2) by Cullen et al. (1978) (see fig. 38). Two clearly separated modes

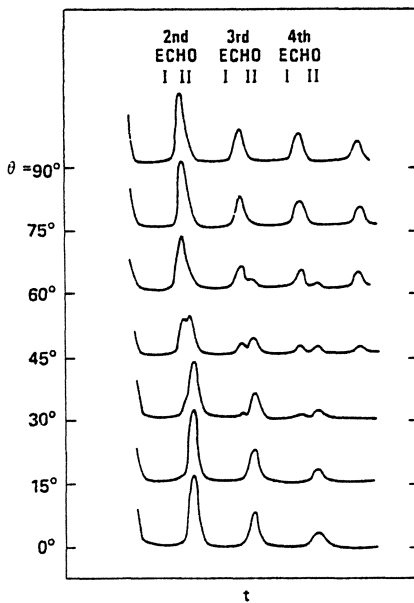


Fig. 37. Echo pattern for shear waves propagating perpendicular to the applied field H in amorphous Tb Fe_2 . The changes in the amplitudes of the peaks as the angle θ between the direction of H and the polarization is varied indicate the presence of two normal modes with polarization parallel and perpendicular to H (taken from Cullen et al. 1978).

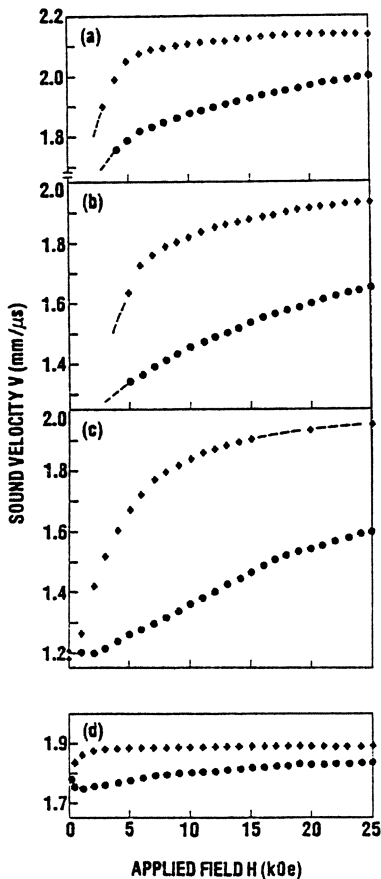


Fig. 38. Sound velocity as a function of applied field H for H parallel and perpendicular to the polarization p (\bullet $H \parallel p$, \blacklozenge $H \perp p$) in (a) $Tb_{0.3}Dy_{0.7}Fe_2$, (b) $Sm_{0.83}Dy_{0.12}Fe_2$, (c) $Sm_{0.7}Ho_{0.3}Fe_2$ and (d) a-TbFe₂ (taken from Cullen et al. 1978).

were observed. The velocity of the slow modes could not be saturated even at 25 kOe. By plotting the velocities of the fast mode vs. $1/H$, the intrinsic (uncoupled) elastic shear moduli, μ^0 , were obtained. The values obtained in this way, along with the values of b_p calculated from the slope of $(\mu^0 - \mu)^{-1}$ vs. H plots are given in table 12.

In the preceding single crystal work it was assumed that $b_2 \gg b_1$. However, $b_1 \neq 0$. In a magnetostrictive system with b_1 and b_2 non-zero, the customary break in the shear degeneracy by the cubic crystal symmetry into the well known normal modes with polarization along the crystalline axes, may not occur. The magnitude and direction of the applied field, as well as the crystal symmetry, determine the normal modes.

TABLE 12

Uncoupled elastic moduli, μ_0 , and magnetoelastic coupling, b_p , for polycrystalline $R\text{Fe}_2$ at room temperature (M_s is in emu/cm³, μ_0 in 10^{11} dynes/cm² and b_p in 10^9 ergs/cm³)*

$R\text{Fe}_2$	M_s	μ_0	b_p
$\text{Tb}_{0.3}\text{Dy}_{0.7}\text{Fe}_2$	780	4.3	1.3
$\text{Sm}_{0.88}\text{Dy}_{0.12}\text{Fe}_2$	360	3.4	1.4
$\text{Sm}_{0.7}\text{Ho}_{0.3}\text{Fe}_2$	145	3.5	0.9
a-TbFe ₂	390	2.9	0.5

* Taken from Cullen et al. (1978).

For the general case of $b_1 \neq 0$ and $b_2 \neq 0$, the expressions for the shear velocities and moduli as a function of field angle θ and magnitude H are given by Rinaldi and Cullen (1978). For propagation along [110] they find

$$v_{\pm}^2 = \frac{1}{2}(C + C') \pm [(\frac{1}{4}(C + C')^2 + B^2)^{1/2}] \quad (7.11)$$

where

$$\begin{aligned} C &= c_{44}^0/\rho - b_2^2 \cos^2 \theta / HM_s \rho \\ C' &= \frac{1}{2}(c_{11}^0 - c_{12}^0)/\rho - b_1^2 \sin^2 \theta / HM_s \rho \\ B &= b_1 b_2 \sin \theta \cos \theta / HM_s \rho \end{aligned}$$

θ is the angle of the applied field with respect to the [001] direction.

If $B = 0$, the two conventional transverse shear waves are polarized along [100] and [110] directions with velocities $C^{1/2}$ and $C'^{1/2}$. When $B \neq 0$, the polarization is determined by the strength of B according to the following expression

$$\tan \Phi_{\pm} = B / [\frac{1}{2}(C' - C) \pm (\frac{1}{4}(C' - C)^2 + B^2)^{1/2}] \quad (7.12)$$

where Φ is the angle of the polarization with respect to the [001] axis.

In fig. 39 are plotted the values of Φ and v vs. the field angle θ for $\text{Tb}_{0.27}\text{Dy}_{0.73}\text{Fe}_2$, taking $b_2 = -2.3 \times 10^9$ ergs/cm³ and assuming $b_1 = 0.1b_2$. Note that the large change in Φ occurs over a small change in θ near $\theta = 45^\circ$ for $H = 8$ kOe. This pulling of the polarization away from the crystal axis has been demonstrated in $\text{Tb}_{0.3}\text{Dy}_{0.7}\text{Fe}_2$ by Cullen et al. (1978).

8. Magnetomechanical coupling of $R\text{Fe}_2$ compounds

Because of their large magnetostriiction the rare earth- Fe_2 compounds have potential as high power transduction elements. In this section the low signal linear properties of these compounds will be examined.

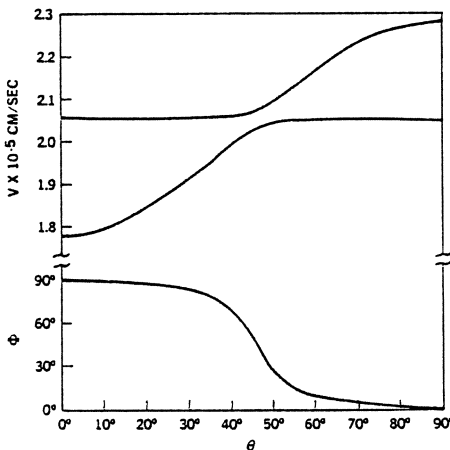


Fig. 39. Calculated dispersion and direction of polarization of one of the shear normal modes vs. the orientation of the magnetization for [110] propagation in Tb_{0.3}Dy_{0.7}Fe₂. The magnetization is in the (110) plane at an angle θ from the [001]. $H = 8$ kOe (taken from Cullen et al. 1978).

The single most important low signal transducer parameter is the magneto-mechanical coupling factor, k . For a magnetomechanical vibrator with no loss or radiation, k^2 denotes the fraction of magnetic energy which can be converted to mechanical (elastic) energy per cycle, or conversely, the fraction of stored mechanical (elastic) energy which can be converted to magnetic energy. For a mechanically driven system $(1 - k^2)E_{\text{el}} = k^2E_{\text{mag}}$. The relation between k^2 and the conventional linear properties of a magnetomechanically coupled system can be obtained starting with the definition of the compliance s^H , permeability μ^T and coupling d through the following equations

$$\epsilon = s^H T + dH \quad (8.1a)$$

$$B = dT + \mu^T H. \quad (8.1b)$$

Here ϵ , B , T and H symbolically represent components of the strain, magnetic induction, stress and magnetic field (see for example Berlincourt et al. 1964). Eliminating T and H respectively from eq. (8.1)

$$B = (d/s^H)\epsilon + \mu^T(1 - d^2/s^H\mu^T)H \quad (8.2a)$$

$$\epsilon = s^H(1 - d^2/s^H\mu^T)T + (d/\mu^T)B. \quad (8.2b)$$

Thus, defining the permeability at constant strain μ^{ϵ} and the compliance at constant induction s^B (blocked conditions), it follows that

$$\mu^{\epsilon} = (1 - d^2/s^H\mu^T)\mu^T \quad (8.3)$$

$$s^B = (1 - d^2/s^H\mu^T)s^H. \quad (8.4)$$

Writing eq. (8.4) in terms of moduli $c \equiv 1/s$

$$c^H = (1 - d^2/s^H \mu^T) c^B. \quad (8.5)$$

In effect, the permeability is reduced from its intrinsic value μ^T whenever energy is transferred to the elastic system. At constant strain the maximum energy is stored in the elastic system. Likewise, the intrinsic (uncoupled) elastic stiffness, c^B , is reduced to a lower value c^H when energy is transferred from the elastic to the magnetic system. Energy is transferred whenever the moment is rotated from its equilibrium value by an applied stress. The maximum fraction of magnetic energy which can be transformed is

$$\frac{\frac{1}{2}\mu^T H^2 - \frac{1}{2}\mu^e H^2}{\frac{1}{2}\mu^T H^2} = \frac{\mu^T - \mu^e}{\mu^T} = \frac{d^2}{s^H \mu^T} = k^2. \quad (8.6)$$

Similarly the maximum fraction of elastic energy which can be transformed is

$$\frac{\frac{1}{2}c^B \epsilon^2 - \frac{1}{2}c^H \epsilon^2}{\frac{1}{2}c^B \epsilon^2} = \frac{c^B - c^H}{c^B} = \frac{d^2}{s^H \mu^T} = k^2. \quad (8.7)$$

The magnetomechanical coupling k is conventionally obtained by measuring the complex impedance of a coil containing the magnetostrictive material. A material coupling factor k_{33} is defined which is geometry independent. For a torroid $k_{33} = k$; for a slender rod $k_{33} \cong (\pi/\sqrt{8})k$. A successful method was developed by Savage et al. (1975) to determine the complex impedance for the low permeability RFe₂ alloys as a function of frequency. The magnetomechanical coupling k_{33} , quality factor Q and permeability μ for Tb_{0.3}Dy_{0.7}Fe₂ calculated this way are shown

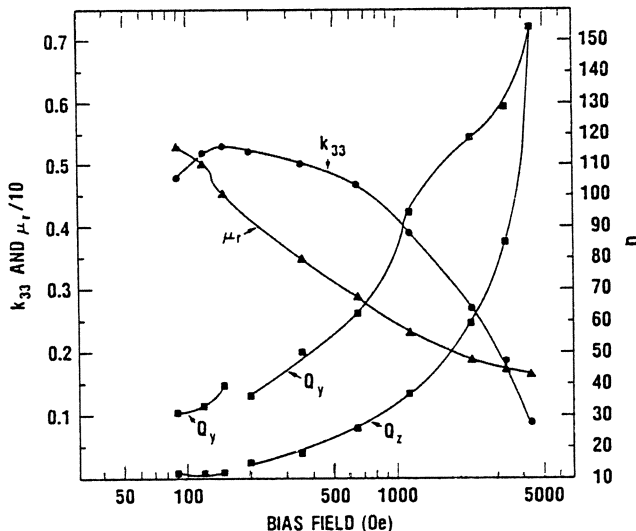


Fig. 40. Coupling factor k_{33} , Q factor and relative permeability μ_r , of Tb_{0.3}Dy_{0.7}Fe₂ as a function of bias field. Q_y , the quality factor at constant current drive, includes both mechanical and electrical losses, whereas Q_z , the quality factor at constant voltage drive, includes only mechanical losses (taken from Savage et al. 1975).

in fig. 40 as a function of magnetic bias. The coupling factor is high when the field is between 100 and 500 Oe. Note that the permeability is low, a necessary consequence of a highly magnetostrictive polycrystal.

In fig. 41 are plotted the resonant and antiresonant frequencies of a 10 cm thin rod of Tb_{0.3}Dy_{0.7}Fe₂ driven magnetically. The resonant frequency differs from the antiresonant frequency at each bias field by an amount related to the coupling. At resonance (maximum change in magnetic induction with fixed magnetic drive H), the bar executes motion at frequency $f^H = v^H/\lambda = (c^H/\rho)^{1/2}/\lambda$, whereas at antiresonance B executes minimum oscillation and the bar vibrates at $f^B = v^B/\lambda = (c^B/\rho)^{1/2}/\lambda$. Thus, from eq. (8.7), neglecting loss terms

$$k^2 = 1 - (f^H/f^B)^2. \quad (8.8)$$

Also, as seen in fig. 41, in a highly magnetostrictive polycrystal both f^B and f^H depend strongly upon applied magnetic field. The change in f^B and f^H with magnetic field reflects the moduli change (ΔE effect) discussed in section 7. It is solely magnetoelastic in origin. The change can be divided into two parts, one macroscopic, due to domain wall motion, and the other microscopic, due to the atomic interaction between the magnetic moment and the local strain field within the domain. In most conventional materials, e.g. Ni, the major contribution arises during the magnetization process by a redistribution of the domains. This induced redistribution due to the pressure field causes a reduction in the modulus. The domain free material at technical saturation is stiffer. Above technical saturation, an externally imposed elastic stress rotates the moment slightly from its aligned condition, allowing the storage of energy in the magnetic system. The amount of rotation depends upon the externally applied field and

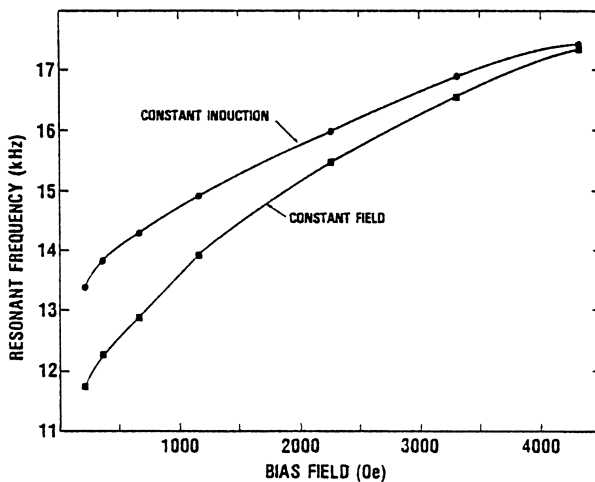


Fig. 41. Resonant frequency (at constant induction and constant field) vs. bias field of a 10 cm bar of Tb_{0.3}Dy_{0.7}Fe₂ (taken from Savage et al. 1975).

any magnetocrystalline anisotropy. Only when the magnetic system is blocked ($H \rightarrow \infty$) is it possible to keep the energy totally within the elastic system and obtain the stiff modulus, c^B . The modulus and ΔE effect at constant field, calculated from f^H for $Tb_{0.3}Dy_{0.7}Fe_2$ is plotted in fig. 33. The increase in modulus is about 150%.

In fig. 42, k_{33} is plotted vs. x for the ternary $Tb_{1-x}Dy_xFe_2$ and $Tb_{1-x}Ho_xFe_2$ alloys. With the addition of $DyFe_2$ and $HoFe_2$ to $TbFe_2$, the values of k_{33} increase to a peak $k_{33} = 0.6$ for $Tb_{0.26}Dy_{0.74}Fe_2$ and $k_{33} \approx 0.44$ for $Tb_{0.25}Ho_{0.75}Fe_2$. Further increases in k_{33} are observed in the quaternary $Tb_xDy_xHo_xFe_2$ system. In table 13, are listed the magnetomechanical coupling factors for a number of rare earth- Fe_2 materials along with those of a few typical magnetostrictive materials. The largest coupling factors are found in grain oriented RFe_2 alloys.

Eddy current losses, which exist in metallic transducers, become important for high frequency applications. In fig. 43 electrical resistivity measurements for $TbFe_2$ are plotted as a function of temperature. At room temperature, its value, while comparable to that of the rare earth elements, is much larger than that of Ni and Fe.

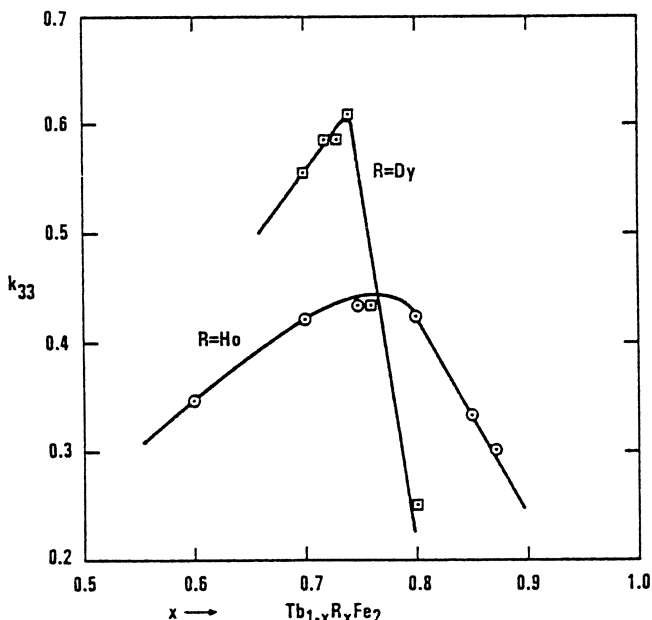


Fig. 42. Magnetomechanical coupling, k_{33} , for $Tb_{1-x}Dy_xFe_2$ and $Tb_{1-x}Ho_xFe_2$ (taken from Savage et al. 1975, Timme 1976).

TABLE I3
Maximum magnetomechanical coupling factor and magnetostriction

	k_{33}	$\lambda_{100} \times 10^6$	$\lambda_{111} \times 10^6$	Reference
Ni	0.31	-51	-23	a, c
13% Al 87% Fe		70	8	b, c
50% Co 50% Fe	0.35	30	160	d, c
4.5% Co 95.5% Ni	0.51	-30	-40	e, f
(NiO) _{0.913} (CoO) _{0.027}				
(FeO) _{0.06} (Fe ₂ O ₃)	0.36	-	-	g
TbFe ₂	0.35	-	2450	h
Tb _{0.3} Dy _{0.3} Fe ₂	0.51	-	1840	h
Tb _{0.27} Dy _{0.73} Fe ₂	0.53-0.60	-	1620	i
Tb _{0.23} Dy _{0.35} Ho _{0.42} Fe ₂	0.61-0.62	-	1130	i
Tb _{0.20} Dy _{0.22} Ho _{0.58} Fe ₂	0.60-0.66	-	820	i
Tb _{0.19} Dy _{0.18} Ho _{0.03} Fe ₂	0.59	-	810	i
SmFe ₂	0.35	-	-2100	h
Sm _{0.88} Dy _{0.12} Fe ₂	0.55	-	-1620	j
Sm _{0.7} Ho _{0.3} Fe ₂	0.35	-	-1370	j
Tb _{0.23} Ho _{0.77} Fe ₂ (oriented)	0.76	-	710	k
Tb _{0.27} Dy _{0.73} Fe ₂ (oriented)	0.74	-	1620	h

^a Bozorth and Hamming (1953).

^b Ferebee and Davis (1958).

^c Hall (1959).

^d Savage and Clark, unpublished.

^e See Davis (1977).

^f Savage et al. (1977).

^g Hall (1960).

^h Savage and Clark (1977).

ⁱ Yamamoto and Nakamichi (1958).

^j Timme, unpublished.

^k Clark (1956).

9. Amorphous RFe₂ alloys

Sputtered alloys of composition RFe₂ are both structurally and magnetically amorphous (see Rhyne et al. 1972). Curie temperatures range from below room temperature to ~ 400 K. A most striking feature of these alloys is the large coercivity at low temperatures (Clark 1973, Rhyne et al. 1974). This is attributed to the combination of high anisotropy and the absence of crystal structure. The maximum energy product calculated for amorphous TbFe₂ at 4 K is 29.5×10^6 GOe, which is comparable to the largest measured value for Sm-Co alloys. While the intrinsically high magnetic anisotropy of the rare earth persists to room temperature, the thermal energy is too high to inhibit magnetization reversal. Consequently coercivities of only ~ 100 Oe are observed at room temperature.

Like the anisotropy, large magnetostrictions are found in the amorphous state (Clark 1973). Forester et al. (1978) have reported magnetostrictions greater than 200×10^{-6} for $0.25 < x < 0.45$ in amorphous Tb_xFe_{1-x}. The room temperature magnetostrictions of amorphous TbFe₂, Tb_{0.3}Dy_{0.7}Fe₂ and DyFe₂ are shown in fig. 44. TbFe₂ has a large unsaturated magnetostriction and DyFe₂ has a spontaneous

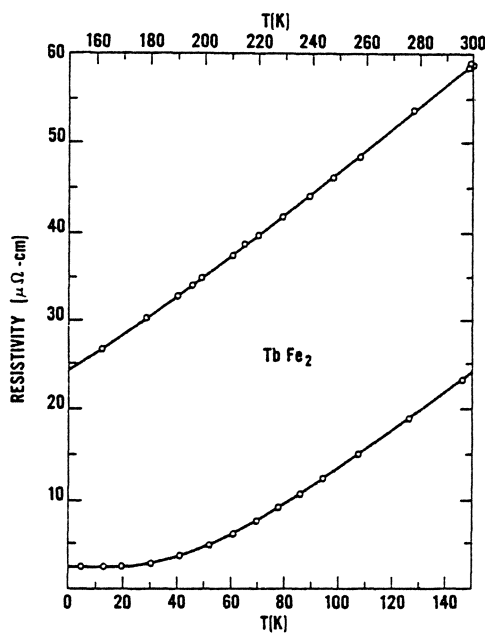


Fig. 43. Resistivity of TbFe_2 vs. temperature (taken from Savage; see Clark 1974).

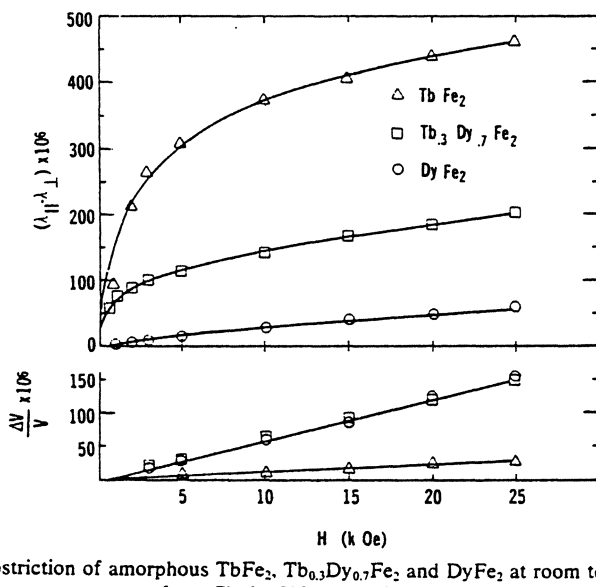


Fig. 44. Magnetostriiction of amorphous TbFe_2 , $\text{Tb}_{0.3}\text{Dy}_{0.7}\text{Fe}_2$ and DyFe_2 at room temperature (taken from Clark 1973, unpublished).

magnetostriction near zero. This difference is accounted for by the difference in Curie temperatures. For amorphous TbFe₂, $T_C >$ room temperature; for amorphous DyFe₂, $T_C <$ room temperature. Unlike crystalline DyFe₂, where $d\lambda/dT < 0$, the magnetostriction of amorphous DyFe₂ increases rapidly with decreasing temperature (fig. 45). Similar to the R Fe₂ compounds, the highly magnetostrictive amorphous alloys can also exhibit a large forced magnetostriction at room temperature.

10. Summary

The R Fe₂ alloys ($R = \text{Sm, Tb, ...}$) derive their magnetostrictive effects from the large anisotropic 4f charge density of the R^{3+} ions. Because of strong Fe-Fe and Fe-R exchange interactions, the large intrinsic zero temperature magnetostriction is preserved more-or-less intact up to room temperature. An unusual magnetostriction anisotropy ($|\lambda_{111}/\lambda_{100}| \gg 1$) characterizes many of these compounds. Thus in polycrystalline materials, the magnetostriction and magnetomechanical coupling is strongly dependent upon crystallite orientation. The high anisotropy of the 4f electron cloud and high Curie temperatures lead to huge cubic magnetocrystalline anisotropies at room temperature as well as large magnetostrains. In TbFe₂ and DyFe₂ the anisotropy is over an order of magnitude larger than that of conventional ferro- and ferrimagnetic cubic materials. The strong magnetoelastic coupling also manifests itself in huge magnetically

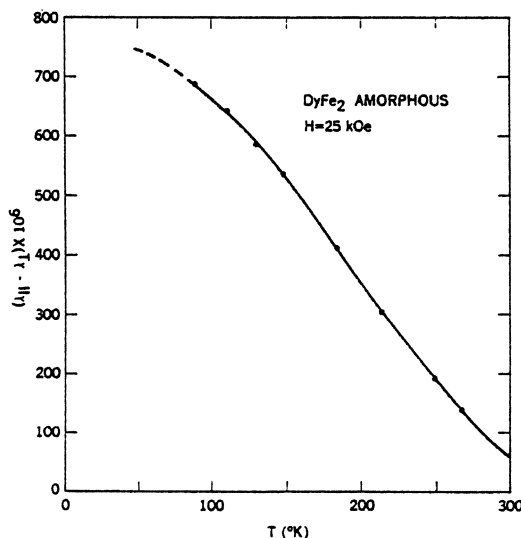


Fig. 45. Magnetostriction of amorphous DyFe₂ vs. temperature (taken from Abbundi and Clark, unpublished).

induced moduli changes. This huge “ ΔE effect” reflects the $|\lambda_{111}/\lambda_{100}| > 1$ anisotropy. Because of the cubic symmetry of the Laves phase $R\text{Fe}_2$ compounds (unlike the hexagonal heavy rare earth elements), the lowest order anisotropy and magnetostriction possess different sign sequences as R is changed from one element to another. Thus pseudobinary $R\text{Fe}_2$ compounds, where R is composed of various rare earths, can be synthesized to exhibit a wide assortment of magnetic properties.

Acknowledgements

The author would like to thank his many co-workers: H.S. Belson, H.T. Savage, J.R. Cullen, R. Abbundi, E. Callen, N. Tamagawa and K. Sato, whose assistance made this chapter possible. Special thanks are due to E. Callen and R. Abbundi for critically reading the manuscript. The author is particularly grateful to N.C. Koon, C.M. Williams, J.J. Rhyne, R.W. Timme and A.E. Miller for many valuable discussions and for permission to include their work prior to publication.

Appendix A: Magnetostriction and magnetic anisotropy of cubic and hexagonal crystals

In computing the crystal field matrix elements for the rare earth ions, $\langle 4f | V_c | 4f \rangle$, the required integrals are of the form: $\int \Psi_{4f} V_l^m \Psi_{4f} d\Omega$. For the rare earths, where $l = 3$, the integrals vanish for $|l'| > 6$. While in many cases it is possible to fit the experimental data with the lowest order magnetostriction constants, e.g. λ_{100} and λ_{111} , within first order perturbation theory we can expect terms to exist up to sixth degree. The proper expression for the magnetostriction for a particular symmetry can be determined by taking the direct product of the basis functions of the same irreducible representation, one function in the strain space and the other in the space of the magnetization. In this way magnetostriction and magnetic anisotropy expressions are generated which not only manifestly reflect the crystal symmetry, but are also orthogonal. Using orthogonal functions has the advantage that the coefficients of the lower order terms do not change as higher order terms are added. In addition, the coefficients of these terms possess characteristic temperature dependences (Callen and Callen 1963).

Expressions for the magnetostriction and magnetic anisotropy to sixth degree in the direction cosines of the magnetization are given below. They are derived from the cubic and hexagonal basis functions of table 1. (Bell 1954).

(a) Cubic:

$$\begin{aligned} \Delta l/l = & \lambda^{\alpha,0} + \lambda^{\alpha,4}\{\alpha_x^4 + \alpha_y^4 + \alpha_z^4 - \frac{3}{5}\} \\ & + \lambda^{\alpha,6}\{\alpha_x^2\alpha_y^2\alpha_z^2 + \frac{1}{21}[\alpha_x^4 + \alpha_y^4 + \alpha_z^4 - \frac{3}{5}] - \frac{1}{105}\} \\ & + \lambda^{\gamma,2}\{\alpha_x^2\beta_x^2 + \alpha_y^2\beta_y^2 + \alpha_z^2\beta_z^2 - \frac{1}{3}\} \\ & + \lambda^{\gamma,4}\{\alpha_x^4\beta_x^2 + \alpha_y^4\beta_y^2 + \alpha_z^4\beta_z^2 - \frac{1}{3}[\alpha_x^4 + \alpha_y^4 + \alpha_z^4] \\ & - \frac{6}{7}[\alpha_x^2\beta_x^2 + \alpha_y^2\beta_y^2 + \alpha_z^2\beta_z^2 - \frac{1}{3}]\} \end{aligned}$$

$$\begin{aligned}
& + \lambda^{\gamma_0} \{ \alpha_x^6 \beta_x^2 + \alpha_y^6 \beta_y^2 + \alpha_z^6 \beta_z^2 - \frac{1}{3} [\alpha_x^6 + \alpha_y^6 + \alpha_z^6] \\
& - \frac{15}{11} [\alpha_x^4 \beta_x^2 + \alpha_y^4 \beta_y^2 + \alpha_z^4 \beta_z^2 - \frac{1}{3} (\alpha_x^4 + \alpha_y^4 + \alpha_z^4)] \\
& + \frac{5}{11} (\alpha_x^2 \beta_x^2 + \alpha_y^2 \beta_y^2 + \alpha_z^2 \beta_z^2 - \frac{1}{3}) \} \\
& + \lambda^{\epsilon_2} \{ \alpha_x \alpha_y \beta_x \beta_y + \alpha_x \alpha_z \beta_y \beta_z + \alpha_z \alpha_y \beta_x \beta_z \} \\
& + \lambda^{\epsilon_4} \{ (\alpha_z^2 - \frac{1}{3}) \alpha_x \alpha_y \beta_x \beta_y + C.P. \} \\
& + \lambda^{\epsilon_6} \{ [\alpha_z^2 - \frac{1}{11} \alpha_z^2 + \frac{1}{33}] \alpha_x \alpha_y \beta_x \beta_y + C.P. \} \\
& + \lambda^{\epsilon_8} \{ [\alpha_x^4 + \alpha_y^4 - \frac{10}{3} \alpha_x^2 \alpha_y^2] \alpha_x \alpha_y \beta_x \beta_y + C.P. \}.
\end{aligned}$$

Note for $l \leq 2$, $\lambda_{100} = \frac{2}{3} \lambda^{\gamma_2}$ and $\lambda_{111} = \frac{1}{3} \lambda^{\epsilon_2}$.

$$\begin{aligned}
E_a = & K^{\alpha_4} \{ \alpha_x^2 \alpha_y^2 + \alpha_y^2 \alpha_z^2 + \alpha_z^2 \alpha_x^2 - \frac{1}{3} \} \\
& + K^{\alpha_6} \{ \alpha_x^2 \alpha_y^2 \alpha_z^2 - \frac{1}{11} (\alpha_x^2 \alpha_y^2 + \alpha_y^2 \alpha_z^2 + \alpha_z^2 \alpha_x^2 - \frac{1}{3}) - \frac{1}{105} \}.
\end{aligned}$$

The conventional cubic anisotropy constants K_1 and K_2 are related to the symmetry constants by $K_1 = -K^{\alpha_4} - \frac{1}{11} K^{\alpha_6}$ and $K_2 = K^{\alpha_6}$.

(b) Hexagonal:

$$\begin{aligned}
\Delta l/l = & \{ \lambda_1^{\alpha_0} + \lambda_1^{\alpha_2} (\alpha_z^2 - \frac{1}{3}) + \lambda_1^{\alpha_4} (\alpha_z^4 - \frac{6}{11} \alpha_z^2 + \frac{3}{33}) \\
& + \lambda_1^{\alpha_6} (\alpha_z^6 - \frac{15}{11} \alpha_z^4 + \frac{5}{11} \alpha_z^2 - \frac{5}{231}) \\
& + \lambda_1^{\alpha_8} (\alpha_x^6 - 15 \alpha_x^4 \alpha_y^2 + 15 \alpha_x^2 \alpha_y^4 - \alpha_y^6) (\beta_x^2 + \beta_y^2) \\
& + \{ \lambda_2^{\alpha_0} + \lambda_2^{\alpha_2} (\alpha_z^2 - \frac{1}{3}) + \lambda_2^{\alpha_4} (\alpha_z^4 - \frac{6}{11} \alpha_z^2 + \frac{3}{33}) \\
& + \lambda_2^{\alpha_6} (\alpha_z^6 - \frac{15}{11} \alpha_z^4 + \frac{5}{11} \alpha_z^2 - \frac{5}{231}) \\
& + \lambda_2^{\alpha_8} (\alpha_x^6 - 15 \alpha_x^4 \alpha_y^2 + 15 \alpha_x^2 \alpha_y^4 - \alpha_y^6) \} \beta_z^2 \\
& + \{ \lambda^{\gamma_2} + \lambda^{\gamma_4} (\alpha_z^2 - \frac{1}{3}) + \lambda^{\gamma_6} (\alpha_x^4 - \frac{6}{11} \alpha_z^2 + \frac{3}{33}) \} \\
& \times \{ \alpha_x \alpha_y \beta_x \beta_y + \frac{1}{3} (\alpha_x^2 - \alpha_y^2) (\beta_x^2 - \beta_y^2) \} \\
& + \{ \lambda^{\gamma_4} + \lambda^{\gamma_6} (\alpha_z^2 - \frac{1}{11}) \} \\
& \times \{ \alpha_x \alpha_y (\alpha_y^2 - \alpha_z^2) \beta_x \beta_y + \frac{1}{8} (\alpha_x^4 - 6 \alpha_x^2 \alpha_y^2 + \alpha_y^4) (\beta_x^2 - \beta_y^2) \} \\
& + \{ \lambda^{\epsilon_2} + \lambda^{\epsilon_4} (\alpha_z^2 - \frac{1}{3}) + \lambda^{\epsilon_6} (\alpha_z^4 - \frac{10}{11} \alpha_z^2 + \frac{5}{33}) \} \\
& \times \{ \alpha_z \alpha_x \beta_x \beta_z + \alpha_z \alpha_y \beta_y \beta_z \} \\
& + \lambda^{\epsilon_8} \{ \alpha_x \alpha_x (\alpha_x^4 - 10 \alpha_x^2 \alpha_y^2 + 5 \alpha_y^4) \beta_z \beta_x + \alpha_z \alpha_y (5 \alpha_x^4 - 10 \alpha_x^2 \alpha_y^2 + \alpha_y^4) \beta_z \beta_y \}.
\end{aligned}$$

$$\begin{aligned}
E_a = & K^{\alpha_2} \{ \alpha_z^2 - \frac{1}{3} \} + K^{\alpha_4} \{ \alpha_z^4 - \frac{6}{11} \alpha_z^2 + \frac{3}{33} \} \\
& + K^{\alpha_6} \{ \alpha_z^6 - \frac{15}{11} \alpha_z^4 + \frac{5}{11} \alpha_z^2 - \frac{5}{231} \} \\
& + K^{\alpha_8} \{ \alpha_x^6 - 15 \alpha_x^4 \alpha_y^2 + 15 \alpha_x^2 \alpha_y^4 - \alpha_y^6 \}.
\end{aligned}$$

Appendix B: Temperature dependences of magnetostriiction and magnetic anisotropy for single-ion models

The magnetostriiction and magnetocrystalline anisotropy of a magnetic system derive from spin operators which have the functional form of the basis functions found in table 1, of section 2 (see Callen and Callen 1963). The temperature

dependences of these quantities depend upon the thermal averages of these operators over the allowed energy states. Thus a calculation of temperature dependences require the quantum statistical averages of such quantities as (Stevens 1952)

$$\begin{aligned} & \langle J_z^2 - J(J+1) \rangle, \\ & \langle 35J_z^4 - 30J(J+1)J_z^2 + 25J_z^2 - 6J(J+1) + 3J^2(J+1)^2 \rangle \quad \text{and} \\ & \langle 231J_z^6 - 315J(J+1)J_z^4 + 735J_z^4 + 105J^2(J+1)^2J_z^2 - 525J(J+1)J_z^2 \\ & \quad + 294J_z^2 - 5J^3(J+1)^3 + 40J^2(J+1)^2 - 60J(J+1) \rangle, \end{aligned}$$

for $l = 2$, $l = 4$ and $l = 6$ respectively. Callen and Shtrickman (1965) have shown that for a large number of theories of ferromagnetism, these averages can be expressed in terms of the moment $\langle J_z \rangle$ itself. These (single-ion) theories include not only molecular field theory, but those collective excitation theories (i.e., spin waves, random field approximation, other Green's function decoupling) in which the quasiparticle levels are equally spaced and ordered like J_z quantum states. In the limit of large J , in the molecular field approximation, these averages take the simple form of the following hyperbolic Bessel functions

$$\begin{aligned} \langle J_z \rangle & \rightarrow \mathcal{L}(x) = -1/x + \operatorname{ctnh} x = m \\ \langle J_z^2 - J(J+1) \rangle & \rightarrow \hat{I}_{5/2}(x) = (3/x^2 + 1) - (3/x) \operatorname{ctnh} x \\ \langle 35J_z^4 \dots \rangle & \rightarrow \hat{I}_{9/2}(x) = (105/x^2 + 45/x + 1) - (105/x^3 + 10/x) \operatorname{ctnh} x \end{aligned}$$

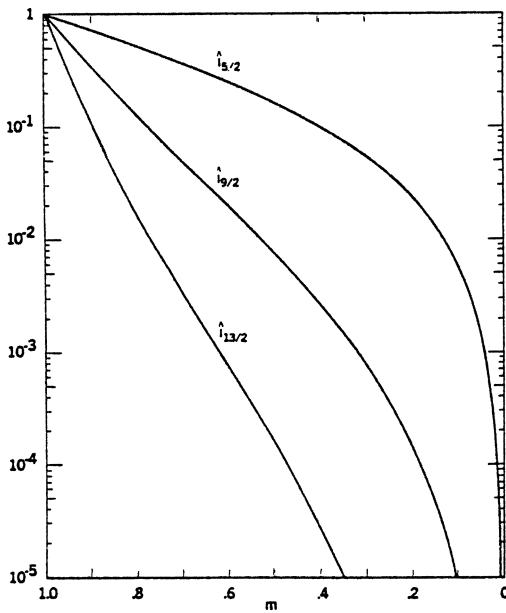


Fig. 46. Normalized hyperbolic Bessel functions $\hat{I}_{5/2}$, $\hat{I}_{9/2}$ and $\hat{I}_{13/2}$ vs. the normalized magnetization, m .

$$(231J_z^6 \dots) \rightarrow \hat{I}_{13/2}(x) = (11 \cdot 945/x^6 + 4725/x^4 + 210/x^2 + 1) \\ - (11 \cdot 945/x^5 + 1210/x^3 + 21/x) \operatorname{ctnh} x.$$

The parameter "x" can be eliminated from these relationships, yielding expressions of the form $\hat{I}_{l+1/2}[\mathcal{L}^{-1}(m)]$ from which eq. (4.3) and eq. (5.1) follow directly.

In fig. 46, $\hat{I}_{5/2}$, $\hat{I}_{9/2}$ and $\hat{I}_{13/2}$ are plotted vs. the reduced magnetization, m . All expressions are normalized to one at $T = 0$ K. From this figure the temperature dependences of the magnetostriction and anisotropy can be directly related to the temperature dependence of the empirically determined magnetization. *The temperature dependences found in this way are independent of the details of the magnetic model.* The hyperbolic Bessel function is a good approximation for the heavy rare earth ions with large J .

References

- Abbundi, R. and A.E. Clark, 1977, IEEE Trans. Mag. MAG-13, 1519.
- Abbundi, R. and A.E. Clark, 1978, J. Appl. Phys. 49, 1969. Also NSWC/WOL/TR 78-88, Naval Surface Weapons Center, Dahlgren, VA 22448, USA; Proc. Int. Conf. on Magnetism ICM-79, Munich, Sept. 1979.
- Abbundi, R., A.E. Clark and N.C. Koon, 1979, J. Appl. Phys. 50, 1671.
- Akulov, N.S., 1928, Z. Physik 52, 389.
- Atzmony, U., M. Dariel, E. Bauminger, D. Lebenbaum, I. Nowik and S. Offer, 1973, Phys. Rev. B7, 4220.
- Atzmony, V. and M. Dariel, 1976, Phys. Rev. B13, 4006.
- Atzmony, V., M. Dariel and G. Dublon, 1977, Phys. Rev. B15, 3565.
- Barbara, B., J. Giraud, J. La Forrest, R. LeMaire, E. Siaud and J. Schweitzer, 1977, Physica 86-88B, 155.
- Bargouth, M. and G. Will, 1971, J. de Physique 32, C1-675.
- Becker, R. and W.D. Doring, 1939, Ferromagnetismus (Springer, Berlin).
- Bell, D.G., 1954, Rev. Mod. Phys. 26, 311.
- Belov, K.P., O.P. Yelyutin, G.I. Katayev, D. Kim, S.A. Nikitin, G.V. Pschenchikova, L.I. Solntseva, G.N. Surovaya, and V.P. Taratynov, 1975, Phys. Met. Metallogr. 39, 50.
- Berlincourt, D.A., D.R. Curran and H. Jaffe, 1964, Physical Acoustics, IA, (by W.P. Mason ed.) (Academic Press, New York).
- Bowden, G., D. St. P. Bunbury, A.P. Guimaraes and R.E. Snyder, 1968, J. Phys. C (Proc. Phys. Soc.) 1, 1376.
- Bozorth, R.M., 1951, Ferromagnetism (Van Nostrand, New York).
- Bozorth, R.M. and R.W. Hamming, 1953, Phys. Rev. 89, 865.
- Bozorth, R.M., E.R. Tilden, and A.J. Williams, 1955, Phys. Rev. 99, 1788.
- Burzo, E., 1971, Z. Angew. Phys. 32, 127.
- Buschow, K. and R. Van Stapele, 1970, J. Appl. Phys. 41, 4066.
- Buschow, K. and R. Van Stapele, 1971, J. de Physique 32, C1-672.
- Callen, E. and H.B. Callen, 1963, Phys. Rev. 129, 578.
- Callen, E. and H.B. Callen, 1965, Phys. Rev. 139, A455.
- Callen, H.B. and S. Shtrickman, 1965, Solid State Comm. 3, 5.
- Chikazumi, S. and S. Charap, 1964, Physics of Magnetism (Wiley, New York).
- Clark, A., 1973, Appl. Phys. Lett. 11, 642.
- Clark, A., 1974, AIP Conf. Proc. No. 18 (American Institute of Physics, New York) p. 1015. Also Proc. 11th Rare Earth Research Conf. (U.S.A.E.C. Tech. INF. Center, Oak Ridge) p. 972.
- Clark, A.E. and H. Belson, 1972, AIP Conf. Proc. no. 5 (American Institute of Physics, New York) p. 1498; Phys. Rev. B5, 3642; IEEE Trans. Mag. MAG-8, 477.
- Clark, A.E. and H.T. Savage, 1975, IEEE Trans. on Sonics and Ultrasonics SU-22, 50.
- Clark, A.E., R. Bozorth and B. DeSavage, 1963, Phys. Lett. 5, 100.
- Clark, A.E., B.F. DeSavage, W. Coleman, E. Callen and H. Callen, 1963b, J. Appl. Phys. 34, 1296.

- Clark, A.E., B. DeSavage and R. Bozorth, 1965, Phys. Rev. **138**, A216.
- Clark, A., H. Belson and N. Tamagawa, 1973a, AIP Conf. Proc. no. 10 (American Institute of Physics, New York) p. 749. Also Phys. Lett. **42A**, 160.
- Clark, A.E., H.S. Belson, and R.E. Strakna, 1973b, J. Appl. Phys. **44**, 2913.
- Clark, A.E., H.S. Belson, N. Tamagawa and E. Callen, 1974, Proc. Int. Conf. on Magnetism ICM-73, Moscow, Sept. 1973, volume IV, p. 335.
- Clark, A., J. Cullen and K. Sato, 1975, AIP Conf. Proc. no. 24 (American Institute of Physics, New York) p. 670.
- Clark, A.E., J. Cullen, O. McMasters and E. Callen, 1976, AIP Conf. Proc. no. 29 (American Institute of Physics, New York) p. 192.
- Clark, A.E., R. Abbundi, O. McMasters and H. Savage, 1977, Physica **86-88B**, 73.
- Clark, A.E., R. Abbundi and W.G. Gillmor, 1978, IEEE Trans. Mag. MAG-14, 542.
- Clark, C.A., 1956, Brit. J. Appl. Phys. **7**, 355; 1961, J. Acoust. Soc. Am. **33**, 930.
- Cullen, J. and A. Clark, 1977, Phys. Rev. **B15**, 4510.
- Cullen, J.R., S. Rinaldi and G.V. Blessing, 1978, J. Appl. Phys. **49**, 1960.
- Davis, C.M., 1977, Proc. Workshop on Magnetostrictive Materials, Naval Research Laboratory, Orlando, Florida, p. 39.
- Dwight, A. and C. Kimball, 1974, Acta. Crys. **B30**, 2791.
- Ferebee, S.F. and C.M. Davis, 1958, J. Acoust. Soc. Am. **30**, 747.
- Forester, D., C. Vittoria, J. Schelleng and P. Lubitz, 1978, J. Appl. Phys. **49**, 1966.
- Freeman, A. and R. Watson, 1962, Phys. Rev. **127**, 2058.
- Guimaraes, A., Ph.D. dissertation. See K.N.R. Taylor, 1971, Adv. in Physics **20**, 551.
- Hall, R.C., 1959, J. Appl. Phys. **30**, 816.
- Hall, R.C., 1960, Trans. TMS-AIME **218**, 268.
- Hoffman, U., 1967, Z. Angew Phys. **22**, 106.
- Keffler, F., 1955, Phys. Rev. **100**, 1692.
- Kittel, C., 1949, Rev. Mod. Phys. **21**, 541.
- Klimker, H., M. Rosen, M.P. Dariel and U. Atzmony, 1974, Phys. Rev. **B10**, 2968.
- Koon, N.C., A. Schindler and F. Carter, 1971, Phys. Lett. **37A**, 413.
- Koon, N.C., A. Schindler, C. Williams and F. Carter, 1974, J. Appl. Phys. **45**, 5389.
- Koon, N.C. and C.M. Williams, 1977, NRL Report 8137, Naval Research Laboratory, Washington, D.C.
- Koon, N.C. and C.M. Williams, 1978, J. Appl. Phys. **49**, 1948.
- Legvold, S., J. Alstad and J. Rhyne, 1963, Phys. Rev. Lett. **10**, 509.
- Masayama, Y., 1931, Sci. Rep. Tohoku Univ. **20**, 574.
- McKeehan, L.W., 1937, Phys. Rev. **51**, 136.
- McMasters, O.D., G.E. Holland and K.A. Gschiedner Jr., 1978, J. Crystal Growth **43**, 577.
- Milstein, J., 1976, AIP Conf. Proc. no. 29 (American Institute of Physics, New York) p. 592.
- Pearson, R.F., 1960, J. Appl. Phys. **31**, 160S.
- Perthel, R., G. Elbinger, and W. Keilig, 1966, Phys. Status Solidi **17**, 151.
- Rhyne, J. and S. Legvold, 1965, Phys. Rev. **138**, A507.
- Rhyne, J., S. Pickart and H. Alperin, 1972, Phys. Rev. Lett. **29**, 1562.
- Rhyne, J., J. Schelleng and N. Koon, 1974, Phys. Rev. **B10**, 4672.
- Rhyne, J., 1978, Handbook on the physics and chemistry of the rare earths, vol. 2 (K. Gschneidner, Jr. and L. Eyring, eds.) (North-Holland, Amsterdam).
- Rinaldi, S., J. Cullen and G. Blessing, 1977, Phys. Lett. **61A**, 465.
- Rinaldi, S., and J.R. Cullen, 1978, Phys. Rev. **18**, 3677.
- Rosen, M., H. Klimker, U. Atzmony and M. Dariel, 1973, Phys. Rev. **B8**, 2366.
- Rosen, M., H. Klimker, U. Atzmony and M. Dariel, 1974, Phys. Rev. **B9**, 254.
- Sato, K., E. Callen and N. Tamagawa, 1976, J. College of Liberal Arts, Toyama University **9**, 19.
- Savage, H.T. and A.E. Clark, Conf. on Rare Earths and Actinides, 1977, Durham, England, July 1977.
- Savage, H.T., A.E. Clark and J. Powers, 1975, IEEE Trans. Mag. MAG-11, 1355.
- Savage, H.T., A.E. Clark, N.C. Koon and C.M. Williams, 1977, IEEE Trans. Mag. MAG-13, 1517.
- Shih, J.W., 1936, Phys. Rev. **50**, 376.
- Smit, J. and H.P.J. Wijn, 1959, Ferrites (Wiley, New York) p. 169.
- Stevens, K.W.H., 1952, Phys. Soc. **65**, 209.
- Timme, R., 1976, J. Acoust. Soc. Am. **59**, 459. Also NRL Report 8064.
- Taylor, K., 1971, Adv. Phys. **20**, 551.

- Tsuya, N., A. Clark and R. Bozorth, 1964,
Proc. Int. Conf. on Magnetism, Nottingham
(Inst. of Phys. and Physical Society, London)
p. 250.
- Wallace, W.E. and E. Skrabek, 1964, Rare
Earth Research II (Gordon and Breach, New
York) p. 431.
- Wallace, W.E., 1968, Prog. Rare Earth Sci.
Technol. 3, 1.
- Wallace, W.E., 1973, Rare earth intermetallics
(Academic Press, New York).
- Weil, L. and K. Reichel, 1954, J. Phys. Radium
15, 725.
- Went, J.J., 1951, Physica 17, 98.
- Wertheim, G., V. Jaccarino and J. Wernick,
1964, Phys. Rev. A135, 151.
- Williams, C. and N. Koon, 1975, Phys. Rev.
B11, 4360.
- Williams, C. and N. Koon, 1977, Physica 86-
88B, 14.
- Williams, C. and N. Koon, 1978, Solid State
Commun. 27, 81.
- Williams, C., N. Koon and J. Milstein, 1978, J.
Phys. Chem. Solids 39, 823.
- Williams, S.R., 1932, Rev. Sci. Instrum. 3, 675.
- Yamamoto, M. and R. Miyasawa, 1965, Sci.
Rep. Tohoku Univ. A5, 22.
- Yamamoto, M. and T. Nakamichi, 1958, J.
Phys. Soc. Japan 2, 228.